



New insights into distinguishing temperate deciduous swamps from upland forests and shrublands with SAR

Sarah Banks^{a,*}, Koreen Millard^b, Laura Dingle-Robertson^a, Jason Duffe^a

^a Environment and Climate Change Canada, 1125 Colonel By Drive, Ottawa, K1A 0H3, Ontario, Canada

^b Carleton University, Department of Geography and Environmental Studies, 1125 Colonel By Drive, Ottawa, K1S 5B6, Ontario, Canada

ARTICLE INFO

Edited by Zhe Zhu

Keywords:

SAR
Wetlands
Swamps
Classification
Change detection
Time series

ABSTRACT

Although wetlands are widely recognized for their important role in providing ecosystem services, their abundance, spatial extent, and condition remain poorly constrained and at-risk of decline. Accurate mapping and monitoring are therefore essential for their protection. However, distinguishing swamps from upland forests and shrublands is especially challenging because optical sensors cannot detect water and/or saturated soil under dense canopies. Synthetic Aperture Radar (SAR) offers distinct advantages in this regard: (1) under certain conditions, microwaves can penetrate vegetation and provide a strong backscattered signal from double bounce when surface water or very wet soil are present, and (2) microwaves can penetrate clouds, providing an opportunity to monitor changes in moisture or the extent of flooding through time. In spite of these advantages, users may still find it difficult to know which wavelengths, incidence angles, polarization states, and times of year can be used to detect swamps because of the complexity of choices, and some confusing and conflicting results presented in the literature. The goal of this research was therefore to better elucidate the impacts of sensor and environmental characteristics on the seasonal backscattering behaviour observed in and separability between swamps and dry, upland forests and shrublands, as well as determine the need for additional ancillary data like digital elevation models and derivatives to improve mapping accuracy. Using SAR data from three sensors with two different wavelengths, various polarization states, and a range of incidence angles we: (1) investigate the drivers of variations in seasonal trends and the frequency and timing of changes among different SAR time series, and assess their impact on separability, (2) quantify the importance of acquisition timing, type, number of derivatives on the accuracy of Random Forest models. Our results show that a common pre-conception that longer wavelengths are preferred for distinguishing flooded versus upland forests and shrublands has proven overly general, that data acquired before leaf flush in the spring provides superior results, and that DEM data only provides an advantage when using sub-optimal SAR data.

1. Introduction

Today it is widely recognized that the level of protection afforded wetlands should better reflect their value to society and the natural environment (Zedler and Kercher, 2005; Mitsch and Gosselink, 2015; Millennium Ecosystem Assessment, 2005; Dugan and Dungan, 1990). However, oftentimes the level of protection permitted is limited by available knowledge on their location, extent, and/or condition. This is especially true of those wetlands densely vegetated by trees (e.g., >6 m in height) and/or shrubs (e.g., 1–6 m in height) (Ministry of Natural Resources and Forestry, 2014), herein referred to as swamps (Riley, 1994; National Wetlands Working Group et al., 1998; Ministry of Natural Resources and Forestry, 2014; Davidson et al., 2022). This is because dense canopies obscure surface saturation and/or flooding from remote detection via aerial photography (Golet and Larson, 1974;

Ministry of Natural Resources and Forestry, 2014), and satellite imagery (Amani et al., 2017; Banks et al., 2019; Pouliot et al., 2019), often resulting in confusion with dry upland forests and shrublands (referred to herein collectively as dry, wooded uplands) that contain the same or similar species and/or densities. Swamps are also difficult to identify because they can occur ephemerally, often drying by late summer, and frequently mark the transition zone between wetlands and uplands (Ministry of Natural Resources and Forestry, 2014).

This presents a significant challenge to establishing unbiased and accurate wetland inventories and monitoring programs since swamps are known to be widely distributed throughout the globe. This includes North America (Davidson et al., 2022) where they are the most common and spatially extensive type of wetland in the conterminous United

* Corresponding author.

E-mail address: sarah.banks@canada.ca (S. Banks).

<https://doi.org/10.1016/j.rse.2024.114377>

Received 8 August 2023; Received in revised form 2 July 2024; Accepted 19 August 2024

Available online 4 September 2024

0034-4257/© 2024 The Authors. Published by Elsevier Inc. This is an open access article under the CC BY license (<http://creativecommons.org/licenses/by/4.0/>).

States (~49% of wetland area (Hall et al., 1994)), Alaska (~76% of the wetland area (Hall et al., 1994)), and parts of Canada (e.g., ~40%–60% of the peatland area in Northern Ontario (Riley, 1994); ~86% of the wetland area in southern Ontario (Byun et al., 2018)) (Tiner et al., 1994; Mitsch and Gosselink, 2015)). Given of the range of ecological settings within which they are found, swamps are also among the most biologically diverse of all wetland types, and are known to provide critical habitat to many regionally rare and at-risk species (Welsch, 1995; Ontario Ministry of Natural Resources and Forestry, 2018). Compared to other treed wetlands (e.g., fens), swamps have higher rates of net primary productivity, below and aboveground biomass, increasing litter input and accumulation of soil organic matter. As a result, they play an important, yet often underappreciated role in the terrestrial carbon cycle (Bona et al., 2018; Stoler and Relyea, 2020; Davidson et al., 2022).

Given the challenge associated with identifying swamps, as well as regional differences in how they are defined, categorized, and mapped (Ministry of Natural Resources and Forestry, 2014; Amani et al., 2017; Banks et al., 2019; Pouliot et al., 2019), their spatial extent and distribution remains highly variable among existing data sources. There are also no established methods or products available for monitoring changes in their hydrology (Davidson et al., 2022). This makes it a challenge to track changes in their health since among all the abiotic factors affecting the function and formation of wetlands, including driving ecosystem processes, hydroperiod (characterizing the frequency and duration of water level perturbations) is the single most important. It is therefore not only critical for determining the presence and extent of swamps, but also their capacity to perform important functions (Lang et al., 2008b; Mitsch and Gosselink, 2015). Given current knowledge gaps, in many models and data sets, including greenhouse gas inventories, swamps are either grouped together with bogs and fens (Kuhn et al., 2021; Olefeldt et al., 2021), or excluded altogether because of a lack of reliable and consistent data (Webster et al., 2018; Bona et al., 2020).

Remote sensors, particularly synthetic aperture radars (SARs), have the potential to improve swamp mapping and monitoring given the capacity of microwaves to penetrate vegetation under certain conditions (Henderson and Lewis, 2008; Bourgeau-Chavez et al., 2009; Corcoran et al., 2013; Amani et al., 2017; Daboor et al., 2019; Banks et al., 2019), and their sensitivity to the presence of surface water and/or soil moisture (Imhoff et al., 1986; Lang et al., 2008a; Townsend, 2002b; Banks et al., 2019). By comparison, shorter wavelength optical sensors are ideal for detecting energy reflected/emitted from the tops of the canopies, especially following leaf-out and/or in the absence of large canopy gaps (Hess et al., 1990; Bourgeau-Chavez et al., 2004; Grenier et al., 2007; Lang et al., 2008a; Bourgeau-Chavez et al., 2009, 2016). With optical sensors, the temporal window within which suitable imagery can be acquired is also restricted to when the atmosphere is free of clouds and/or haze, making it more challenging to acquire images coincident with seasonal flooding and/or soil saturation.

At the same time, defining the conditions that permit canopy penetration and produce detectable differences in SAR backscatter and/or phase remains a challenge (Magagi et al., 2002). This is because these conditions vary based the complex interaction among several variables, including: (1) sensor characteristics (e.g., polarization, frequency, resolution, noise floor, incidence angle), and (2) environmental conditions (e.g., moisture content, size, shape, number, and/or orientation of gaps in the canopy, trunks, stems and leaves, and tree height, extent of flooding, surface roughness of the ground/water, dielectric properties of the soil, understory vegetation). It is unsurprising then that varying levels of success have been reported on the use of SAR for identifying and monitoring changes in swamps (Townsend, 2001, 2002b; Lang et al., 2008a; Henderson and Lewis, 2008; Amani et al., 2017; Daboor et al., 2019; Banks et al., 2019).

This raises questions regarding the cause and degree to which accuracies can vary for classification and change detection products based

solely on differences in the SAR data being acquired, and whether environmental conditions vary through space and time. Left unexplained, the value of such products is diminished as this can lead to reporting errors and confusion among end users. There is therefore a need to not only improve image interpretation, but also quantify potential biases, especially since: (1) SAR data are becoming more widely available, free, and open, (2) SAR data vary in terms of their quality, and information content with respect to a given application, (3) the number and diversity of SAR sensors and data types continues to increase, and (4) there is increasing demand for and capacity to generate global products that are challenging to calibrate to or validated for all possible data types and environmental conditions. Given the widespread use of Digital Elevation Models and their derivatives to improve wetland mapping accuracy (Millard and Richardson, 2013; Mahdavi et al., 2018; Banks et al., 2019; White et al., 2017; Pontone et al., 2024), there is also a need to determine the relative importance of these data given they represent nearly time-invariant information. When ultimately driving a model's predictive performance then, they are not well-suited for assessing changes through time (e.g., in wetland extent) (Banks et al., 2019).

2. Objectives

The goal of this research was therefore to better elucidate the impact of sensor and environmental characteristics on the intraannual backscattering behaviour observed in and the separability between, swamps and dry, wooded uplands, as well as determine the need for additional ancillary data, like DEMs and derivatives, to improve mapping accuracy. To this end, multiple SAR time series were acquired over the same study area to: (1) investigate the drivers of variations in seasonal trends and the frequency and timing of changes among different SAR time series, and assess their impact on separability, and (2) quantify the importance of acquisition timing, type, number of SAR derivatives, and the availability of DEM information, on the accuracy of Random Forest models.

The rest of the manuscript is organized as follows. Section 3 describes the theory of microwave interactions in swamps and dry, wooded uplands, and provides a summary of the various sensor and environmental characteristics that affect both the transmissivity of the canopy and backscatter from the ground and/or water surface. Section 4 describes the methods, and the results and discussion are in Sections 5 and 6. Limitations are reported in Section 6, and the conclusions are provided in Section 7.

3. Background

3.1. Theoretical model of SAR backscatter from swamps and dry, wooded uplands

From wooded areas (wet or dry), SAR backscatter is the coherent sum of electromagnetic waves from multiple scattering interactions, including: (1) single scattering events, producing returns directly from the trunk layer, ground/water, and/or canopy, and (2) scattering attributable to multiple interactions between the ground/water surface, trunk layer, and/or canopy (e.g., trunk to ground/water surface and vice versa) (Ormsby et al., 1985; Imhoff et al., 1986; Richards et al., 1987; Dobson et al., 1995; Wang et al., 1995; Townsend, 2002b; Kasischke and Bourgeau-Chavez, 1997; Ahern et al., 2018). Relative differences in returns from all sources vary widely, even for SAR data acquired with the same sensor characteristics, because of differences in environmental conditions.

Among these differences, it is the presence and/or absence of surface water that has a significant affect on backscattering behaviour and therefore the separability between swamps and dry, wooded uplands. When incident upon the ground/water surface, some fraction of the transmitted microwave signal is transmitted to lower layers and usually

absorbed and/or converted to heat energy, while the remainder is reflected. When incident upon a smooth surface (measured relative to the wavelength of incident microwaves) all incoming radiation is scattered forward at an angle equal to the incidence angle and measured from normal on the intercepting surface to parallel with the radar line of sight. As surface roughness increases scattering becomes more diffuse as the beamwidth of the scattered radiation spreads but remains centered in the same, specular direction (Ahern et al., 2018).

When a swamp is completely flooded then its ground/water surface is smooth so much of the incident signal is preserved and directed away from the radar antenna. A large proportion of this can then be redirected back toward the sensor from other forward scattering events: (1) double bounce, where the incident signal interacts with two surfaces oriented at some angle to another (i.e., the trunk and ground/water surface), and (2) multi-path, where multiple scattering interactions occur (i.e., between the ground/water surface, trunk and/or canopy) (Imhoff et al., 1986; Wang et al., 1995; Kasischke and Bourgeau-Chavez, 1997). As a result, returns are often higher from swamps than dry, wooded areas for which a greater proportion of the transmitted microwave signal is transmitted and absorbed by lower layers of the soil and/or diffused by rough features (e.g., hummocks, live and/or senescent vegetation) (Engheta and Elachi, 1982; Imhoff et al., 1986; Townsend and Walsh, 2001; Townsend, 2002b; Brisco et al., 2013; White et al., 2015; Dabboor et al., 2019).

Polarimetric radars can also measure the co-pol phase difference representing the inter-channel phase between HH and VV (electric field vector oscillates perpendicularly (H) or parallel (V) to the direction of travel for both incident (first letter) and received (second letter) polarizations). This information can then be used to identify different scattering mechanisms. This includes double bounce as there is usually a change in the orientation (direction of oscillation from down to up or vice versa) of the vertically, but not the horizontally polarized wave, resulting in a phase shift of up to 180° following two scattering events. However, research has demonstrated that it can be less reliable when acquired at steep incidence angles and/or under dry conditions (Brisco et al., 2015, 2017; Ahern et al., 2018; Atwood et al., 2020; Ahern et al., 2022). In such cases, other indicators of double bounce, especially high returns in the HH polarization, or a high HH to VV ratio are preferred.

3.2. Sensor and environmental characteristics affecting the effective transmissivity of the canopy and returns from the water/ground surface and trunks

Given this model of the backscattering behaviour observed within swamps and dry, wooded uplands, there is need to understand the sensor characteristics and environmental conditions affecting differences in contributions from single or multiple scattering events. More specifically, it stands to reason that the capacity to differentiate swamps from dry, wooded uplands with SAR is predicated on the fact that incident microwaves are capable of penetrating the intervening canopy and trunk layers (Wang et al., 1995; Townsend, 2001; Lang et al., 2008a,b; Bourgeau-Chavez et al., 2016; Banks et al., 2019). This is because when incident microwaves predominately interact with the tops of canopies, their backscatter and phase can be indistinguishable between wet or saturated and dry areas, especially when vegetation types and/or densities are similar (Townsend, 2002b; Amani et al., 2017). Moreover, in the absence of standing water at the surface, the extent to which incident microwaves are preserved and redirected also depends on the moisture content of the soil, while the density of vegetation within the understory also affects the degree of signal attenuation.

The following therefore aims to provide a summary of both the sensor and environmental characteristics known to affect the effective transmissivity of the canopy (measured relative to the characteristics of the microwaves transmitted by the sensor, as well as the environmental conditions of the wetland being imaged) and scattering at the water and/or ground surface in both swamps and dry, wooded uplands.

3.2.1. Wavelength

As wavelength decreases (frequency increases) relative to the average diameter of structural elements within the canopy, generally, so too does the attenuation depth and penetration capacity of the radar signal (Woodhouse, 2017). As a result, the branches and/or leaves of shrubs and trees can be effectively transparent to longer wavelength (e.g., P- (30–100 cm) and L-(23 cm) band) microwaves, while penetration of shorter (e.g., C-(5.7 cm) and X-(3.5 cm) band) wavelength microwaves can be greatly reduced, especially in densely vegetated areas. Because of this, results from studies that have used longer wavelength (e.g., L-band data) SARs for inundation mapping in wooded areas have been more consistently positive (Ormsby et al., 1985; Place, 1985; Krohn et al., 1983; Gesch, 1990; Hess and Melack, 1994; Townsend and Walsh, 1998; Costa et al., 1998; Townsend and Walsh, 1998) compared to shorter wavelength (e.g., C-band) SARs (Hess et al., 1995; Wang et al., 1995; Moreau et al., 1998; Townsend and Walsh, 1998; Milne et al., 2000; Henderson and Lewis, 2008; Amani et al., 2017). Though there are some exceptions (Banks et al., 2019), this has led to a prevailing notion that longer wavelengths are required to detect flooding and/or soil saturation in forests and shrublands.

3.2.2. Incidence angle

The angle of incidence at which a radar image is acquired can also impact the effective transmissivity of the canopy and relative roughness of the ground surface. Generally, as incidence angle increases, so too can attenuation within the canopy as this increases the path length between the sensor and surface, increasing the number of features with which the signal interacts (Richards et al., 1987; Ford and Casey, 1988; Hess et al., 1990; Kandus et al., 2001; Magagi et al., 2002). This can effectively limit returns originating from the ground and/or water surface, so it is similarly well-established that steeper angles (i.e., 20–30° Hess et al., 1990; Sokol et al., 2004; Lang et al., 2008b) are generally preferred for detecting surface saturation and/or flooding in wooded areas, especially when there is a range of different cover types (Richards et al., 1987; Hess et al., 1990; Wang et al., 1995; Wang and Imhoff, 1993; Bourgeau-Chavez et al., 2001). However, some authors have also reported that results were not affected by incidence angle (e.g., Ormsby et al. (1985) and Imhoff et al. (1986) with SIR-B L-band data, and Townsend and Foster (2002) with Radarsat-1 C-HH data acquired between 10 to 46°).

3.2.3. Polarization and polarimetric diversity

The polarization of the transmitted signal also affects the detectability of surface saturation and/or flooding in the presence of woody vegetation. HH, especially if acquired at long wavelengths (e.g., L-band) (Hess et al., 1995; Hess and Melack, 2003), is generally considered the best single polarization for penetrating vegetation (Wang et al., 1993; Bourgeau-Chavez et al., 2001; Townsend, 2002a). By comparison, greater signal attenuation and increased scattering of vertically polarized microwaves occurs before incident signals can reach the ground and/or water surface due to the presence of vertically oriented trunks and other vegetation (Hess et al., 1995; Wang et al., 1995). This is especially true with shorter wavelength C-band data, for which it has been demonstrated that VV can be much less effective for identifying flooding in wooded areas (Wang et al., 1995; Townsend, 2002b). At longer wavelengths, the impact of polarization can be less significant, as both L-band cross (HV/VH) and VV polarized data have been useful for identifying swamps, though are generally not as good as HH (Schmullius and Evans, 1997). Many authors have also found that use of multiple polarizations can improve separability between flooded and non-flooded forests (Henry et al., 2006; Horritt et al., 2003; Banks et al., 2019), and can be more sensitive to wetland plant phenology and changes in hydrology (Dabboor et al., 2019).

3.2.4. Vegetation structure and phenology

The physical structure of the vegetation (e.g., number, size and configuration of branches and leaves) and its condition (e.g., moisture content), can also affect the attenuation depth and penetration capacity of incident microwaves (Richards et al., 1987). Generally, the more open the canopy (Lang et al., 2008b), and when the wavelength is much greater than leaf size (Pope et al., 1994; Wang et al., 1995), there is greater potential to detect surface saturation and/or flooding, even with C-band (Townsend and Walsh, 1998; Rao et al., 1999; Townsend, 2001, 2002a; Costa, 2004; Lang et al., 2008b) VV data (Townsend and Walsh, 1998). In many cases, the transmissivity of the crown also changes throughout the growing season and is greatest prior to the leaf-out. At this time a range of wavelengths, incidence angles, and polarizations have been used to detect surface water and/or saturated soils in wooded areas (Townsend, 2002b; Lang et al., 2008a; Amani et al., 2017; Banks et al., 2019), even with X-band data (Voormansik et al., 2013).

Once transmitted through the canopy, the ground and/or water surface and vegetation in the understory can also impact the detectability and capacity to monitor changes in surface water and/or soil moisture in wooded areas. This includes the transmissivity of the trunk layer, surface roughness, and the number and diameter of trunks (Lang et al., 2008a). In cases where vegetated hummocks cover a significant portion of the ground surface, for example, it is expected that incident microwaves are more diffused, possibly to an extent which renders observed backscatter indiscriminate from dry, wooded uplands. The size and number of trunks also determines the strength of the returned signal. With too few trunks, or trunks that are much smaller in size than the wavelength of incident microwaves, returns may be low despite the presence of saturated soil and/or flooding. In such cases, shorter wavelengths may be preferred (Townsend, 2002b).

3.3. Noise and sensitivity

Even in cases where incident microwaves can effectively penetrate the canopy, a sensor's radiometric sensitivity or resolution ultimately dictates its capacity to distinguish between targets, especially if similar in value and low in intensity (Woodhouse, 2017; Dabboor et al., 2019; Banks et al., 2019). With SARs, contributions from noise are typically quantified in terms of a Noise Equivalent Sigma Zero (NESZ) value, representing the equivalent radar cross section required to produce a signal-to-noise ratio of 1 (i.e., an equal proportion of noise and received signal) (Woodhouse, 2017). A higher (worse) noise floor therefore yields a lower signal to noise ratio, increasing the range of values observed for a given target and diminishing a sensor's capacity to distinguish between targets with similar returns. Though the effects of noise are reduced when returns are higher, they can still impact the separability of classes like swamps and dry, wooded uplands (Banks et al., 2019).

3.4. Summary and impetus for this work

In addition to some of the conflicting results noted above, it is notable that users do not always have the flexibility to select among different wavelengths, incidence angles, polarizations, and/or noise floors. Depending on their access, or extent of their area of interest, many can only use what is free and open given the high cost and limited spatial and/or temporal coverage of some sensors. As a result, it is often necessary to sacrifice data quality and/or information content for coverage and/or availability. This is another reason why further study is needed on the extent to which sensor parameters and/or environmental conditions may bias results, and whether such biases can be reduced with additional ancillary data.

4. Methods

4.1. Study area

The study area is located in Prince Edward County, an island roughly 60 km wide, along the northern shore of Lake Ontario, Canada (approx. 44°1'20.39"N, 77°14'50.27"W). Found within the Manitoulin-Lake Simcoe ecoregion, the site is characterized by mild winters and warm summers, with a mean annual temperature of approximately 6 °C (mean winter temperature is -4.5 °C and mean summer temperature is 16.5 °C). Here, precipitation levels remain constant throughout the year, totalling between 750–1000 mm annually. Agricultural land is the dominant cover type, though mixedwood forest makes up a high proportion of the landscape. Topographic variations are relatively subtle, and there are many wetlands, though swamp is the most common and spatially extensive (Banks et al., 2019). Here, and throughout all of southern Ontario, swamps contain mostly deciduous species (Bunting et al., 1998) and can vary widely in terms of the range of species within a given stands, the density of trees and/or shrubs, the moisture content of the soil, and extent of flooding and/or exposure of soil and/or hummocks (Table 1).

4.2. Water level measurements

To assess the rate and magnitude of seasonal changes in water level in swamps, measurements were taken at two sites using two Solinst Levelogger Edge (model 3001) sensors encased in stilling wells (Fig. 1). Each instrument recorded the hydraulic head at 15-minute intervals. Values were then corrected by compensating for the effects of atmospheric pressure using one of two barometers installed at the northern and southern parts of the study area (i.e., using the barometer in closest proximity). As shown in Fig. 1, although rain was recorded throughout the growing season, water levels recorded within swamps decreased throughout the growing season. Drying trends were also observed throughout the study area during multiple site visits (Banks et al., 2019).

4.3. SAR imagery and processing details

Four SAR time series were acquired over the study area (Table 2), including multi-angle, quad-pol Radarsat-2, and coherent dual-pol Sentinel-1 and Alos-2. Compared to Sentinel-1, the availability of both Radarsat-2 and Alos-2 data was more limited as both satellites require tasking, neither were free and open at the time they were acquired, and because of the longer time interval (repeat pass) when images can be acquired with the exact same geometry (incidence and look angle): 24 days for Radarsat-2 and 14 days for Alos-2, versus 12 days for Sentinel-1. Each SAR image was processed using the same method, as follows. First, images were stored in the scattering matrix format, expressed in sigma nought (linear power) (Cloude and Pottier, 1996). Each image was then boxcar filtered (using a 5 × 5 pixel window) to reduce the effects of speckle, then converted to the 3 × 3 coherency (C3) and covariance (T3) matrices (Radarsat-2 data only) or 2 × 2 covariance (C2) matrix (Sentinel-1 and Alos-2) (Cloude and Pottier, 1996). While represented in slant range geometry, the Freeman–Durden decomposition (Freeman and Durden, 1998) and phase difference between HH and VV was calculated for the Radarsat-2 images (Banks et al., 2019; White et al., 2015, 2017). Note that because of the Brewster Angle effects, power contributions attributed to double bounce were expected to be underestimated for the Radarsat-2 FQ5 W image, though were still considered potentially suitable for detecting relative differences between swamps and dry, wooded uplands (Ahern et al., 2018). Each multi-band raster was then orthorectified using the Rational Functions model based on definitive orbit information and a high resolution Digital Elevation Model (final pixel spacing and estimated equivalent number of looks (ENL) (Anfinson et al., 2009), provided in Table 2) (Banks et al., 2019).

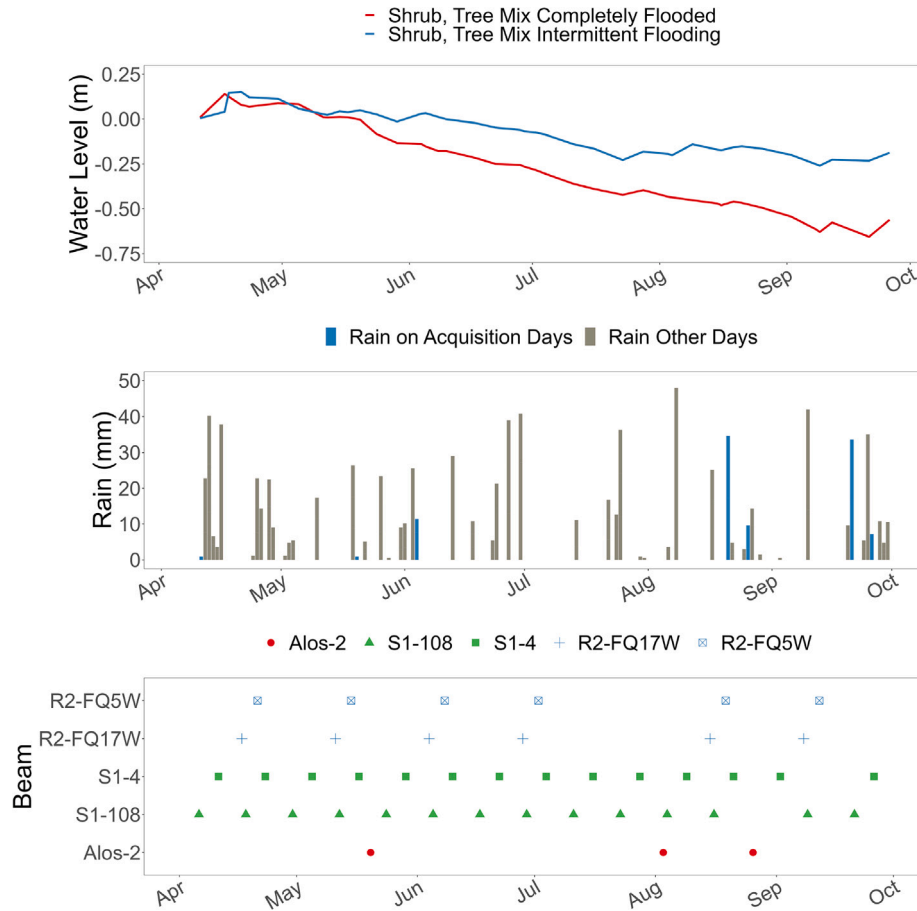


Fig. 1. Seasonal changes in water level for two swamps with the initial water elevation measured at each site on the first day removed from all subsequent dates for display purposes (top), daily rainfall (middle), and the timing of each acquisition (bottom).

4.4. Analysis

Classification results from a previous study were used to mask other land cover types in the area, including agricultural fields, water, marshes, and shallow water wetlands and other land covers from further analysis (Banks et al., 2019). 400 point samples were then generated for both swamps and dry, wooded uplands (800 total) by: (1) randomly distributing point vectors throughout the entire study area, all of which were field-verified, and (2) by randomly distributing point vectors within manually digitized polygons (Banks et al., 2019). All points were spaced at least 50 m apart in an attempt to account for the effects of spatial autocorrelation (Millard and Richardson, 2015), and for each point, raster values of all images and bands, for each time series, were extracted and used to address the objectives as follows.

4.4.1. Variations in seasonal trends, frequency and timing of change

Box and whisker plots were used to display the range of values of SAR derivatives for each class and used in combination with the omnibus test statistic and its factorization (Conradsen et al., 2003, 2016) to analyse variations in (1) seasonal trends, and (2) the frequency and timing of changes between SAR time series. Data collected in the field (Banks et al., 2019) was then used to identify the factors influencing these variations, and assesses their impact on separability to address the first objective.

Change was evaluating using the omnibus test statistic since it has already been used to quantify the impact of various SAR sensor characteristics on the number and timing of statistically significant changes

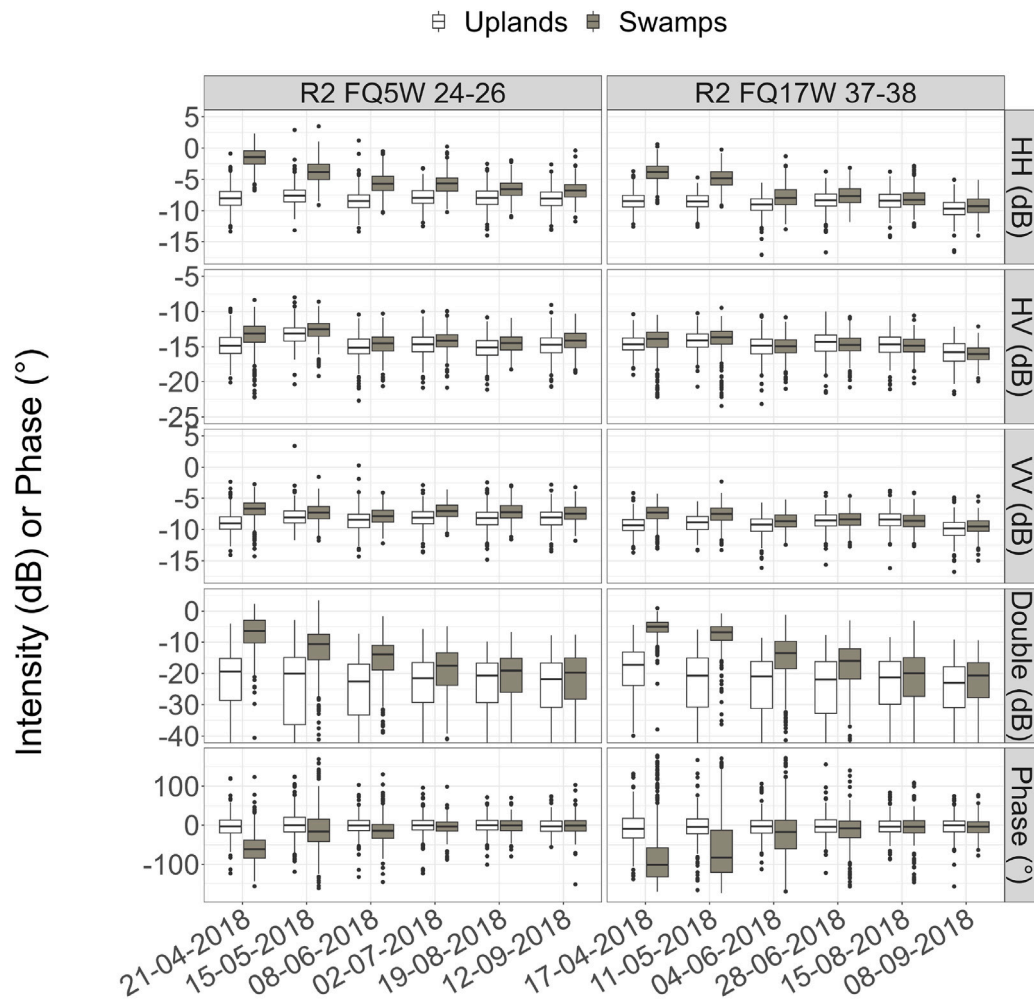
between SAR time series (Dabboor et al., 2019), and has proven effective for detecting short-term, seasonal changes in swamps (Dabboor et al., 2019) and other wetland types (Muro et al., 2019, 2016).

The omnibus test detects pixel-wise changes within a stack of k uncorrelated and multi-looked coherency or covariance matrices (i.e., all images in each of the four SAR time series). Compared to pairwise methods that can be less sensitive to gradual change, the omnibus approach evaluates change across all possible combinations of pairs. It also takes into consideration that values for both C and T are known to follow a complex Wishart distribution, providing a basis for which change can be assessed and evaluated on the basis of statistical significance (Conradsen et al., 2003). Against all alternative hypotheses (change) then, the null hypothesis (no change) is tested using the parameters that characterize each distribution and using the omnibus statistic (i.e., $H_0 : \Sigma_1 = \Sigma_2 = \dots = \Sigma_k$) as follows:

$$Q = \left[k^{2k} \frac{\prod_i^k = 1 |c2_i|}{|C2|^k} \right]^n \quad (1)$$

where $C2 = \Sigma_i^k = 1c2_i$ and n is the number of looks. Values of the latter reflect the accuracy with which the distribution Q is estimated at each pixel. Approximate values for Q are provided in Conradsen et al. (2016) and Q test statistic can also be factorized following (Conradsen et al., 2016) to determine the time interval in which change occurs.

Following preparation of T3 (Radarsat-2 time series) and C2 (Sentinel-1 and Alos-2 time series) matrices the Docker image mort/sardocker was used to: (1) estimate the ENL of each SAR dataset (samples focused on dry, wooded uplands at the peak of the growing



Acquisition Timing (DD-MM-YYYY)

Fig. 2. Seasonal trends of select SAR derivatives for each Radarsat-2 time series.

season, for which speckle statistics were expected to be fully developed), (2) co-register images to a reference (i.e., the first image in each time series), and (3) apply multi-temporal change detection to identify the timing of the first, and number of changes (significance level set to 95%). Note that the use of statistical significance is essential to separate differences in backscatter attributable to real change versus differences that are attributable to speckle and noise (Canty, 2024).

4.4.2. Image classification

To address the second objective, multiple classification scenarios were tested using Random Forest in R (Breiman, 2001; Liaw et al., 2002). Random Forest was used given its ubiquity within remote sensing (Belgiu and Drăguț, 2016) and other fields, as well as its ease of implementation and interpretation. To compare models, independent accuracy assessments were performed, and variable importance was calculated based on the Shapley value (Shapley, 1997; Nandlall and Millard, 2019). Random Forest's own internal measures of importance were not used as they are known to be biased in the presence of correlated variables (Genuer et al., 2010), and variables that differ in scale (Strobl et al., 2007).

For all scenarios (Table 3 and described subsequently) the same classifier settings were used (1000 trees; the default value of *mtry* - the number of variables randomly selected to determine the optimal split at each node Millard and Richardson, 2015; White et al., 2017;

Banks et al., 2019; Millard et al., 2020). To account for variations between model runs attributable to the subset of training/validation used in constructing models, accuracies were averaged across 100 bootstrapped iterations of each scenario (i.e., using the same classifier settings and inputs, but a different random sample for training (70%) and independent validation (30%)) (see Table 3).

First, intensity values from single images (one date) were classified, then intensity values from two different dates, for all possible two-date combinations, were classified (Table 3) as previous studies have shown that multi-temporal data can improve classification accuracies (Banks et al., 2019). With the Radarsat-2 time series, an additional set of models were run that included phase-based derivatives (Table 3, column 2). A DEM and two derivatives (Topographic Wetness Index and slope Banks et al., 2019) were then added to each single and two-date models (Table 3).

For each modelling scenario Shapley values were calculated to quantify the relative importance or contribution of individual and/or grouped variables (players) to the accuracy of each modelling scenario (cooperative game where the goal is to maximize accuracy) (Nandlall and Millard, 2019). For each player, a higher Shapley value indicates a greater contribution to overall accuracy, and the sum of each player's Shapley values (for a specific game) is equal to the overall accuracy (Nandlall and Millard, 2019).

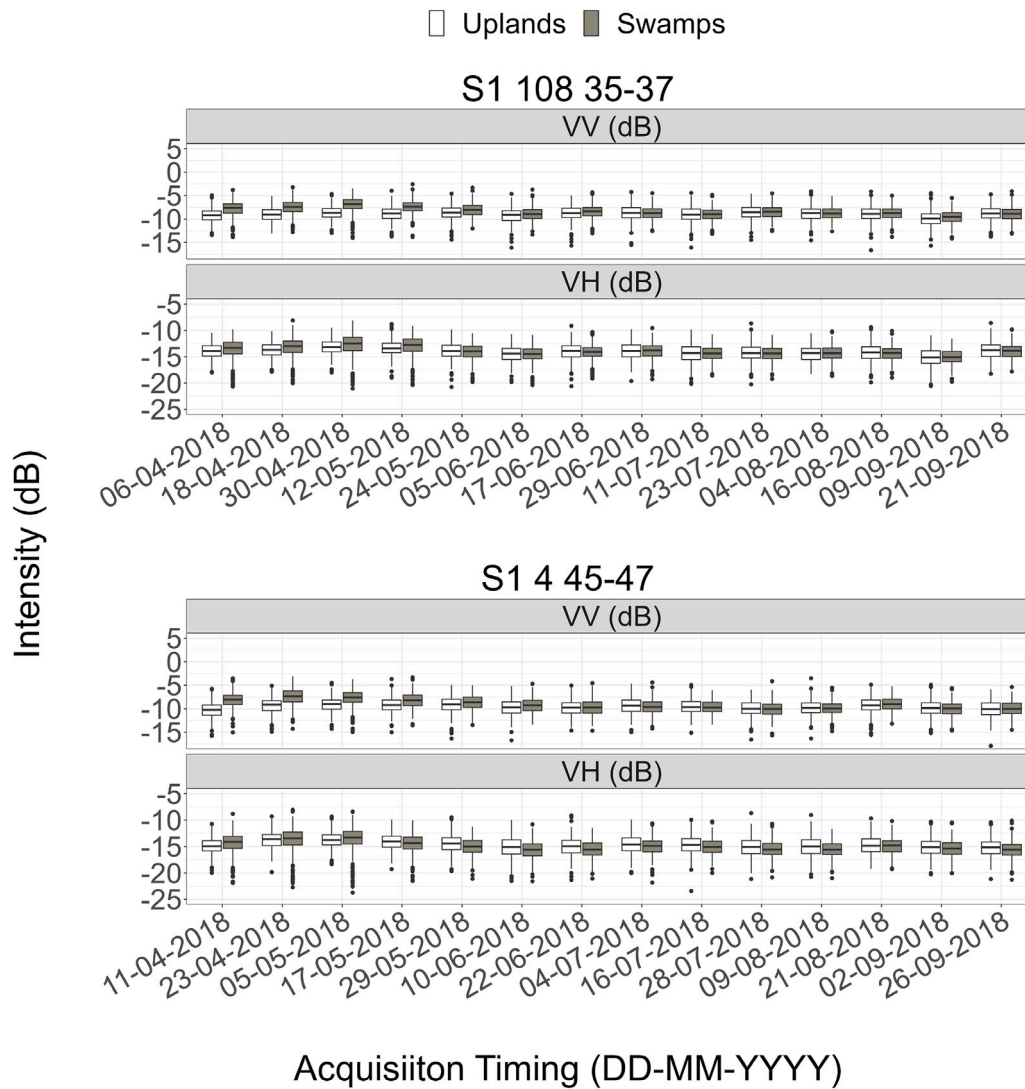


Fig. 3. Seasonal trends of Sentinel-1 VV and VH intensity values for each time series.

5. Results

5.1. Variations in seasonal trends, frequency and timing of change

Early in the growing season, preceding both the leaf out of the canopy and a decrease in water levels (after mid-May), backscattering returns from swamps exceeded those from dry, wooded uplands in all SAR time series (Fig. 2). This is due to the high transmissivity of the canopy at that time (i.e., leaf off) and higher double bounce scattering. Evidence of this includes high returns attributable to double bounce from the Freeman–Durden decomposition (Radarsat-2 time series), high HH returns (Radarsat-2 and Alos-2 time series), a high HH to VV ratio (Radarsat-2 time series), and the difference in relative phase between HH and VV (Radarsat-2 time series). Cross-pol (HV or VH) returns at C-band (Radarsat-2 and Sentinel-1 time series) were also higher for swamps early in the growing season, while at L-band, HV returns were similar for both classes. This difference reflects the lower sensitivity of longer wavelength microwaves to fine-scale features (e.g., branches of trees or shrubs), that typically yield high cross-pol returns at C-band, especially in the presence of surface water (Ullmann et al., 2016, 2017; Banks et al., 2019).

Given differences in scattering behaviour, separability between swamps and dry, wooded uplands was also high early in the growing season, though decreased significantly through time and varied widely

among both SAR sensors and derivatives (Figs. 2, 3 and 4). Surprisingly, the R2 FQ5 W 24–26 HH intensity image acquired on April 21st offered the best separability among all SAR derivatives even compared to the Alos-2 41–43 HH intensity image acquired on May 20th (7 versus 70% of the 800 samples (400 per class) occupied a common range (Figs. 2 and 4)). This is a result of the combined effects of the lower NESZ value of the R2 FQ5 W 24–26 image, as well as its acquisition at a steep angle which reduced canopy attenuation and resulted in higher returns. These yielded a higher signal to noise ratio, reducing the range of values for swamp compared to Alos-2 (i.e., minimum and maximum HH intensities spanned 9 dB versus 14 dB with the Alos-2 41–43 HH image acquired on May 20th). Even when compared the R2 FQ5 W 24–26 HH intensity image acquired on April 15th, just five days before the earliest Alos-2 image and following canopy leaf out in some areas (Table 1), fewer samples for swamp and dry, wooded uplands occupied a common range (58 versus 70%). Separability was also higher between swamp and dry, wooded uplands with the two earliest FQ17 W HH intensity images than the earliest Alos-2 image (just 27 and 46% of class samples occupied a common range), though was not as high as the earliest R2 FQ5 W 24–26 HH given they were acquired both later in the growing season (following leaf out in some areas) and at shallower angles, which resulted in more canopy attenuation. For all Radarsat-2 HH images acquired between June and September separability was lower, though similar to the Alos-2 images acquired in August.

Table 1

Types of swamps found throughout the study area. Photos are of representative samples taken approximately parallel to the radar line of sight of the Fine Quad-Pol Wide Radarsat-2 images between May 14–18th, 2018 (Table 2). Flooding conditions were recorded at the same time, thus reflect conditions in spring.

Type	Description	Photos
Shrub, Tree mixed completely flooded in spring	Mix of tall maple and elm trees, and a thick understory of dogwoods, grasses, and reeds. No exposed land and/or hummocks.	
Shrub, Tree mixed intermittent flooding in spring	Living and dead maple trees, red osier dogwood, and green ash. Understory intermittently flooded, with dense vines, hummocks of soil, grasses, reeds, and moss.	
Treed — Intermittent flooding in spring	Dense stands of tall trees, mostly silver maple, and birch. Open understory with intermittent flooding and some areas of exposed soil and herbaceous plants.	
Treed — Completely flooded in spring	Mostly silver maple, with an open understory of mostly water, with few hummocks of exposed ground, grasses, and reeds.	

Though less separable with the Sentinel-1 time series due to the availability of sub-optimal polarizations (VV and VH), a higher (worse) noise floor, and images being acquired at shallower angles than the R2 FQ5 W 24–26 images (Fig. 3), VV returns were still higher on average in swamps than dry, wooded uplands early in the growing season. This difference suggests dissimilarities in scattering at the ground/water surface. As noted previously, in the presence of flooding incident microwaves are mostly redirected from the smooth water surface to vertically oriented trunks, which can then be returned back in the

Table 2

SAR time series (DD-MM-YYYY) and final, processed image specifications (in the table R2 = Radarsat-2, S1 = Sentinel 1, A2 = Alos-2). Listed below the table for each time series is the final pixel spacing, incidence angle, polarization, look direction, and estimated ENL. Note that Radarsat-2 FQ numbers (5 and 17) and Sentinel-1 relative orbit numbers (4 and 108), denote images acquired with different incidence angles and resolutions based on the side looking geometry of the sensor.

	R2 FQ5 W 24–26 ^a	R2 FQ17 W 37–38 ^b
Radarsat-2	21-04-2018	17-04-2018
	15-05-2018	11-05-2018
	08-06-2018	04-06-2018
	02-07-2018	28-06-2018
	19-08-2018	15-08-2018
	12-09-2018	08-09-2018
Sentinel-1	S1 108 35–37 ^c	S1 4 45–47 ^d
	06-04-2018	11-04-2018
	18-04-2018	23-04-2018
	30-04-2018	05-05-2018
	12-05-2018	17-05-2018
	24-05-2018	29-05-2018
	05-06-2018	10-06-2018
	17-06-2018	22-06-2018
	29-06-2018	04-07-2018
	11-07-2018	16-07-2018
	23-07-2018	28-07-2018
	04-08-2018	09-08-2018
16-08-2018	21-08-2018	
09-09-2018	02-09-2018	
21-09-2018	26-09-2018	
A2 41–43 ^e	20-05-2018	03-08-2018
		26-08-2018

- ^a 8 m, 24–26°, quad-pol, ascending, 17.
- ^b 8 m, 37–38°, quad-pol, descending, 17.
- ^c 10 m, 35–37°, VV+VH, ascending, 15.
- ^d 10 m, 45–46°, VV+VH, ascending, 15.
- ^e 10 m, 41–43°, HH+HV, ascending, 15.

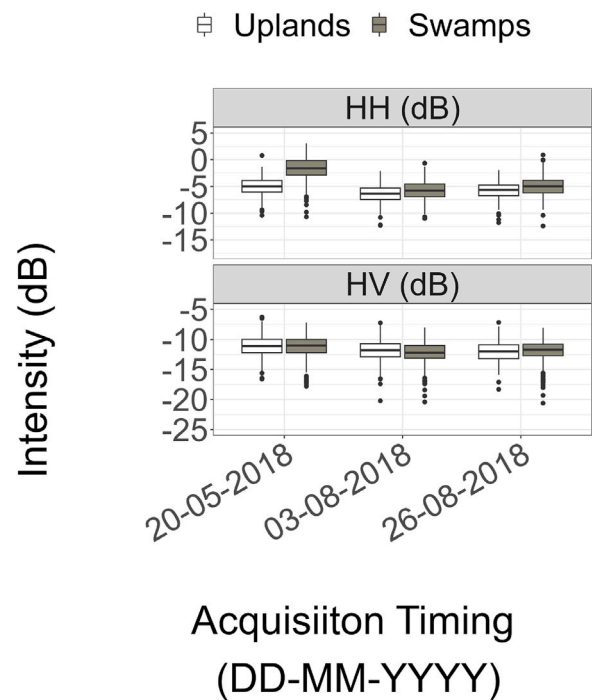


Fig. 4. Seasonal trends of Alos-2 HH and HV intensity values.

direction of the sensor. In dry uplands however, a larger proportion of the signal can be diffused when incident upon rough features at the

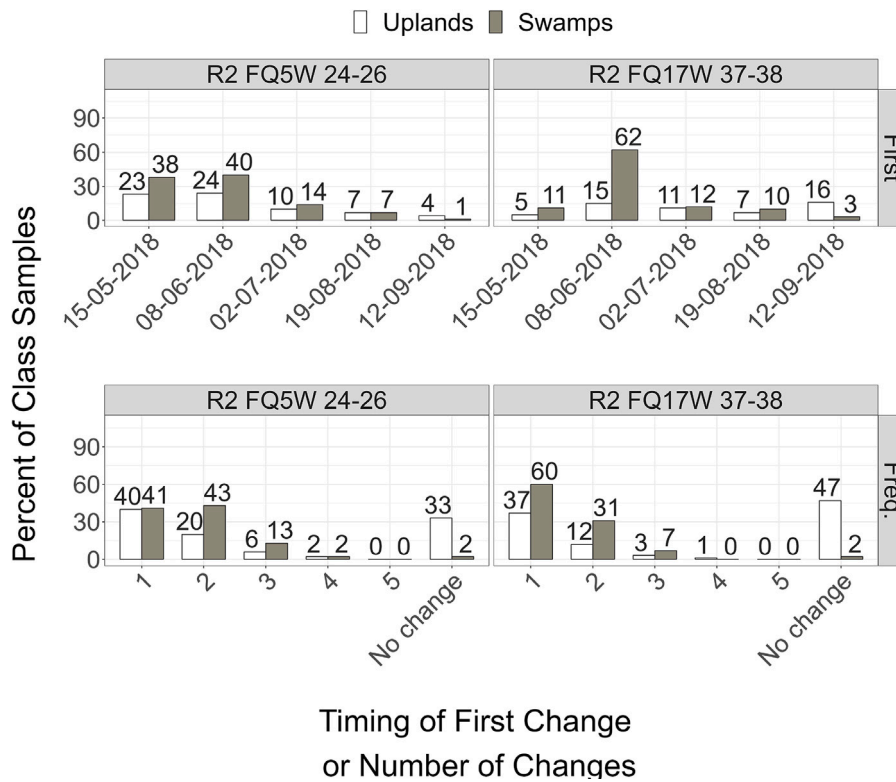


Fig. 5. Change detection results (as a percentage of the 400 samples for each class) for the Radarsat-2 time series indicating the timing of the first and total number (freq.) of statistically significant changes (rounded to the nearest integer). X-axis labels indicate the timing (acquisition date) or number of changes (or “no change”, if applicable).

Table 3

Classification scenarios tested for each SAR time series (Table 1), and based on backscatter intensity alone (I), backscatter intensity and phase information (P), and I and/or P combined with a DEM (DEM). This series of tests was completed for both all single dates and all possible two-date combinations. Numbers indicate the number of models run for each time series, which varied depending on the number of images available.

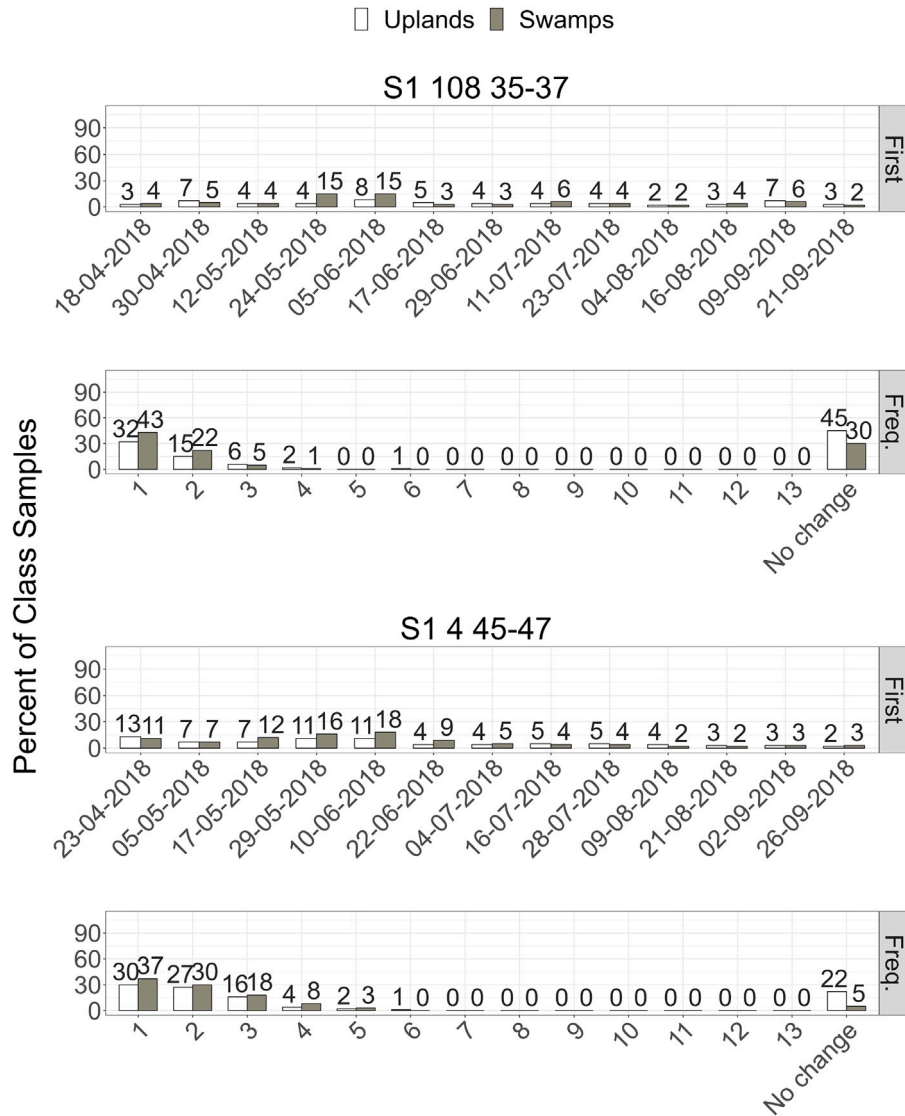
	I	I+P
Single dates	R2 FQ5 W 24–26 (6)	R2 FQ5 W 24–26 (6)
	R2 FQ17 W 37–38 (6)	R2 FQ17 W 37–38 (6)
	S1 108 35–37 (14)	
	S1 4 45–47 (14)	
	A2 41–43 (3)	
Two dates	R2 FQ5 W 24–26 (15)	R2 FQ5 W 24–26 (15)
	R2 FQ17 W 37–38 (15)	R2 FQ17 W 37–38 (15)
	S1 108 35–37 (91)	
	S1 4 45–47 (91)	
	A2 41–43 (3)	
Single dates	I+DEM	I+P+DEM
		R2 FQ5 W 24–26 (6)
	S1 108 35–37 (14)	R2 FQ17 W 37–38 (6)
	S1 4 45–47 (14)	
	A2 41–43(3)	
Two dates		R2 FQ5 W 24–26 (15)
		R2 FQ17 W 37–38 (15)
	S1 108 35–37 (91)	
	S1 4 45–47 (91)	
	A2 41–43 (3)	

surface, explaining why returns were lower in dry, wooded uplands than in swamps, and thus why VV offered some separability between classes.

As the growing season progressed, separability decreased for all SAR time series, though change detection results showed that this was a result of different environmental factors (Figs. 5, 6 and 7). With the

Alos-2 time series, change was not detected in a majority of the samples for dry, wooded uplands (93%) despite both the both the leaf out of the canopy (Fig. 1) and growth of vegetation in the understory (identified during field visits). Again, this is a reflection of the decreased sensitivity of L-band microwaves to fine scale changes in the vegetation that are known to affect scattering behaviour at C-band (Figs. 5 and 6) (Dabboor et al., 2019). In swamps though, change was detected in 67% of samples, most of which occurred between the first (May 20th) and second (August, 3rd), acquisition, were a result of a decrease in HH returns, and led to a majority of class samples occupying a common range (i.e., 98%; Fig. 4). Given water levels decreased during this time (Fig. 1) this underscores the critical role of the presence and/or absence of surface water in the separability between swamps and dry, wooded uplands at L-band. More specifically, while canopy leaf out may not have affected backscattering behaviour, an absence of surface water in swamps resulted in backscattering returns that were indistinguishable from dry, wooded uplands.

With both the Radarsat-2 and Sentinel-1 time series change was detected in more samples for dry, wooded uplands (53%–78% versus 7% with Alos-2) and in many cases coincided with the timing of the leaf out of the canopy around mid-May (Figs. 1, 5 and 6). This is a result of the increased sensitivity of shorter wavelength, C-band microwaves to fine scale changes in plant growth and phenology. However, it is notable that with the R2 FQ5 W 24–26 time series, dry, wooded uplands and swamps still remained separable with data collected on May 15th despite the leaf out of the canopy in some areas yielding a statistically significant change in 23 and 38% of samples for each class between April 21st and May 15th (Fig. 5). Compared to the Radarsat-2 time series, it is notable that Sentinel-1 change detection results were more challenging to interpret since, more acquisitions were available, increasing the likelihood of images being collected under a wider range of environmental conditions (e.g., during or immediately preceding rainfall; Fig. 1).



Timing of First Change or Number of Changes

Fig. 6. Change detection results (as a percent of the 400 samples for each class) for the Sentinel-1 time series indicating the timing of the first and total number (freq.) of statistically significant changes (rounded to the nearest integer). X-axis labels indicate the timing (acquisition date) or number of changes (or “no change”, if applicable).

5.2. Image classification and variable importance

5.2.1. Single dates

The accuracy of Random Forest models based on derivatives from single SAR images (dates) varied not just based on sensor characteristics (e.g., incidence angle, polarization, noise floor, but acquisition timing (Figs. 8 and 9)). With both Radarsat-2 time series, model accuracy was higher early in the growing season before leaf-out, then decreased. With the R2 FQ5 W 24–26 data this decrease was more gradual (96, 87, 78, 73, 66, to 64%), while a more obvious step change was observed with the R2 FQ17 W 37–38 time series following leaf out (96, 93, 68, 61, 51, 51%). This step change was similarly observed in the trend analysis, and change detection results and shows that compared to the R2 FQ5 W 24–26, accuracies were more affected by the leaf out of the canopy, and less by changes in water level.

At similar times in the growing season, the accuracies of models constructed with the Sentinel-1 and Alos-2 time series were lower than those based on Radarsat-2 data (Fig. 9). For example, the average overall accuracy for the R2 FQ5 W 24–26 image acquired on 21-04-2018 was of 96% compared to just 69% for the S1 108 35–37 image acquired three days earlier on 18-04-2018. In some cases though differences were relatively minor. For example, the average overall accuracy for the R2 FQ5 W 24–26 image acquired on 15-05-2018 was just 3% higher than the A2 41–43 image acquired on 20-05-2018 (i.e., 87 vs. 84%).

Considering the best models for each time series though, the highest accuracy achieved with Radarsat-2 data (96%) was 21 and 12% higher than the best Sentinel-1 (75%) and Alos-2 (84%) models. To be clear, this demonstrates that optimally timed acquisitions, even if acquired at shorter wavelengths, can perform equally as well as long-wavelength

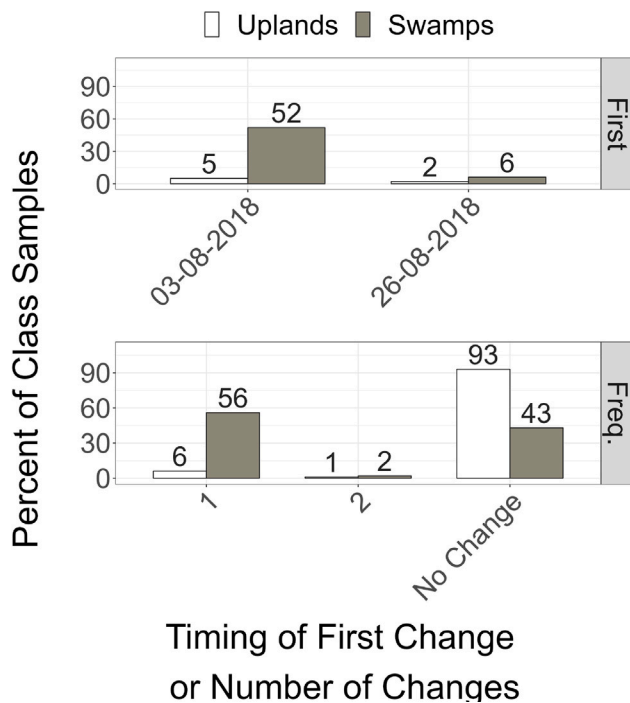


Fig. 7. Change detection results (as a percentage of the 400 samples for each class) for the Alos-2 time series indicating the timing of the first and total number (freq.) of statistically significant changes (rounded to the nearest integer). X-axis labels indicate the timing (acquisition date) or number of changes (or “no change”, if applicable).

L-band SAR for separating swamps and dry, wooded uplands, though requires that the data are acquired with a low (better) noise floor and in the optimal (HH) polarization.

Shapley values confirm the importance of the HH polarization to overall accuracies, especially early in the growing season for both the Radarsat-2 and Alos-2 time series (Fig. 8). By comparison, contributions from HV or VH and VV were lower, and similar through time with the Radarsat-2 time series, while VV tended to contribute more early in the growing season with the Sentinel-1 data. Models based on the Radarsat-2 time series also show that phase information had a minimal impact on model accuracy, as in most cases differences between models based on intensity versus intensity and phase did not exceed 3%.

Including the DEM and its derivatives (topographic wetness and slope) also had a variable impact on the accuracy of Random Forest models. For example, accuracies remained high and unchanged for models based on early season data, though increased for models constructed with late-season data. The relative importance of the DEM and its derivatives was also proportionally higher in models based on SAR images acquired later in the growing season. For example, values increased from 27 vs. 36% with the earliest and latest R2 FQ5 W 24–26 images (Fig. 8). Nearly all models, regardless of sensor, acquisition characteristics, or acquisition timing, achieved accuracies exceeding 75% with the inclusion of the DEM and its derivatives. This demonstrates the potential for these data to compensate for differences in accuracies that may arise from varying sensor and environmental characteristics.

5.2.2. Two dates

For Random Forest models constructed with derivatives from two SAR images (two dates), accuracies similarly varied by sensor characteristics and acquisition timing (Figs. 10 and 11). With both Radarsat-2 time series the average overall accuracy of models ranged from 62%–97% with those constructed with derivatives from one or more images acquired early in the growing season achieving the highest accuracies,

while those constructed with derivatives from images acquired late in the growing season achieving the lowest accuracies. However, many models’ accuracies exceeded those achieved for single dates, even if acquired following the leaf out of the canopy. This similarly demonstrates capacity to compensate for the effect of acquisition timing through inclusion of multiple acquisition dates, though returns diminished as images were acquired later into the growing season following leaf out, and potentially the drying of some swamps.

By comparison, the best Sentinel-1 and Alos-2 models based on derivatives from two SAR images (dates) were 82 and 89%, 15 and 8% less than the best Radarsat-2 models (97%), and only 5 and 4% better than the best Sentinel-1 and Alos-2 models based on derivatives from one SAR image (date). This indicates that, like with the Radarsat-2 data, multi-temporal Sentinel-1 and Alos-2 data only marginally improved upon the accuracy of models constructed with derivatives from single SAR images acquired at the optimal time in the growing season (i.e., prior to leaf out). At the same time, for the Sentinel-1 time series, multiple models based on derivatives from two images achieved accuracies 75%, while the accuracy of all models based on derivatives from single images where 75% or less.

Shapley values demonstrate the relative importance of images acquired early in the growing season, especially when the second image was acquired much later (Figs. 10 and 11). For example, with the R2 FQ5 W 24–26 time series, all models constructed with derivatives from the image acquired on 21-04-2018 equalled 97%, though contributions from these derivatives increased from 53 to 64% when combined with derivatives from images acquired on 15-05-2018, 08-06-2018, 02-07-2018, 19-08-2018, and 12-09-2018, respectively. Shapley values were also more similar for derivatives from images acquired either before or after the leaf out of the canopy.

Including the DEM and its derivatives had a similar impact on Random Forest models constructed with derivatives from two SAR images. Accuracies remained high for models constructed with early season data, though increased for images acquired later in the growing season (i.e., by up to 15, 27, and 17% with the Radarsat-2, Sentinel-1, and Alos-2 time series). For models constructed with SAR images acquired later in the growing season, the relative importance of the DEM and its derivatives was also proportionally higher, increasing from 27–34, 27–39, 32–43, 24–34, and 32%–40% for the best to worst two-date combinations from the R2 FQ5 W 24–26, R2 FQ17 W 37–38, S1 108 35–37, and S1 4 45–47, and Alos-2 time series, respectively.

6. Discussion

Our findings emphasize the need for a more nuanced understanding of the impact of both environmental and SAR sensor characteristics on the capacity to detect flooding and/or soil saturation in wooded areas. The prevailing consensus that longer wavelengths are better suited for detecting flooding and/or soil saturation (Richards et al., 1987; Hess et al., 1995; Wang et al., 1995) has proven overly general. Rather, both sensor and environmental characteristics together determine the extent to which: (1) incident microwaves can penetrate to the ground/water surface, and (2) whether returns are enhanced and/or produce detectable differences to which the sensor is sufficiently sensitive to. Herein, several observations have been made that support this conclusion, including: (1) the trend analysis showed that among all SAR derivatives, the C-band R2 FQ5 W 24–26 HH intensity offered the best separability late into the growing season, and (2) the classification results demonstrated the importance of acquisition timing, the benefit of HH polarized data, and of a better noise floor over longer wavelength L-band Alos-2 data.

The impact of acquisition timing on the accuracy of Random Forest models in particular, cannot be understated. Interestingly, as long as the image was acquired early in the growing season accuracies were relatively high among all SAR sensors, polarizations, and incidence angles, regardless of whether ancillary data like DEMs and

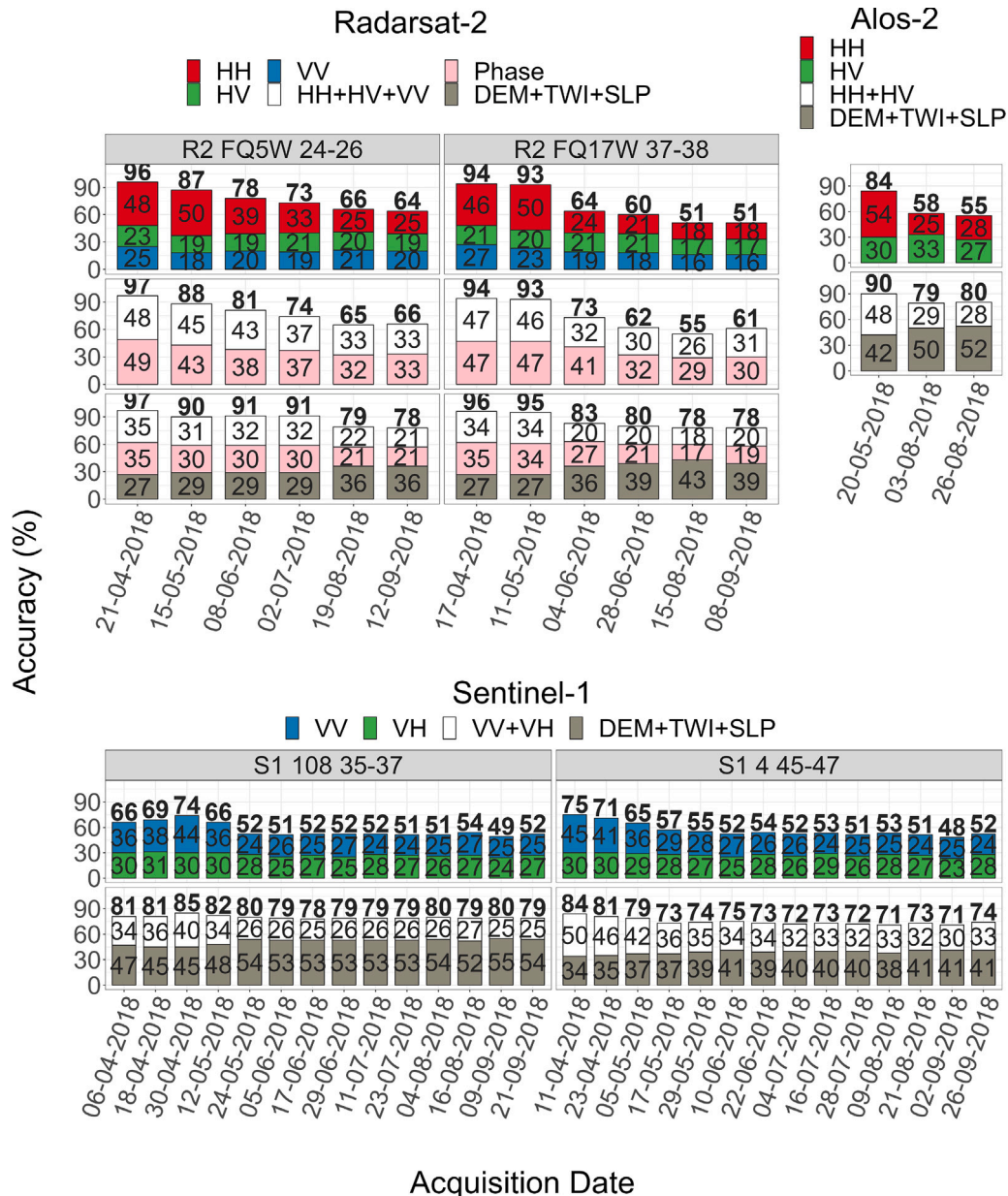


Fig. 8. Shapley values for single (HH, HV, VH or VV polarization) and grouped sets of variables (by SAR image acquisition date and by DEM, topographic wetness index (TWI) and slope (SLP) together) to demonstrate their relative importance to the independent overall accuracy (total bar height) of multiple Random Forest models (averaged across 100 runs). Shown above are all models based on single SAR images (dates) classified alone (top row) and with a DEM plus derivatives (bottom row). Shapley values are summed above each bar to indicate the independent overall accuracy of each model.

their derivatives were included. Other authors have reported similar findings when attempting to distinguish swamps from dry, wooded uplands. Townsend (2001), for example, found accuracies decreased from 98% to 89% when classifying leaf-off and leaf-on C-band Radarsat-1 imagery. Lang et al. (2008a) saw accuracies fall by 7%–10% when they classified leaf-on C-band ASAR imagery. Banks et al. (2019) also found that classification accuracies decreased by 11 to 21% when classifying leaf off vs. leaf-on C-band Radarsat-2 and simulated C-band Radarsat Constellation Mission data over the same study site. Notably, map products based on early season data are expected represent the maximum extent of swamps which vary dramatically between years. Long-term monitoring may therefore be required to distinguish sites that are only flooded because of a single high water event, though do

not meet the definition of a wetland (Ministry of Natural Resources and Forestry, 2014).

These results also highlight that when captured in a transitional state, or unknowingly before or after some phenological and/or hydrologic event, significant changes in scattering behaviour can occur. As a result, classifiers may perform unpredictably in areas containing swamps and dry, wooded uplands, based solely on the timing of when the data was collected. Moreover, even if acquired at the optimal time in the growing season, results may still be significantly biased because of the polarization and noise floor of the sensor. Herein, we have demonstrated that this bias can be reduced by including multiple dates and/or other ancillary data like DEMs and their derivatives. However, it is notable that these and other biases may not always be readily

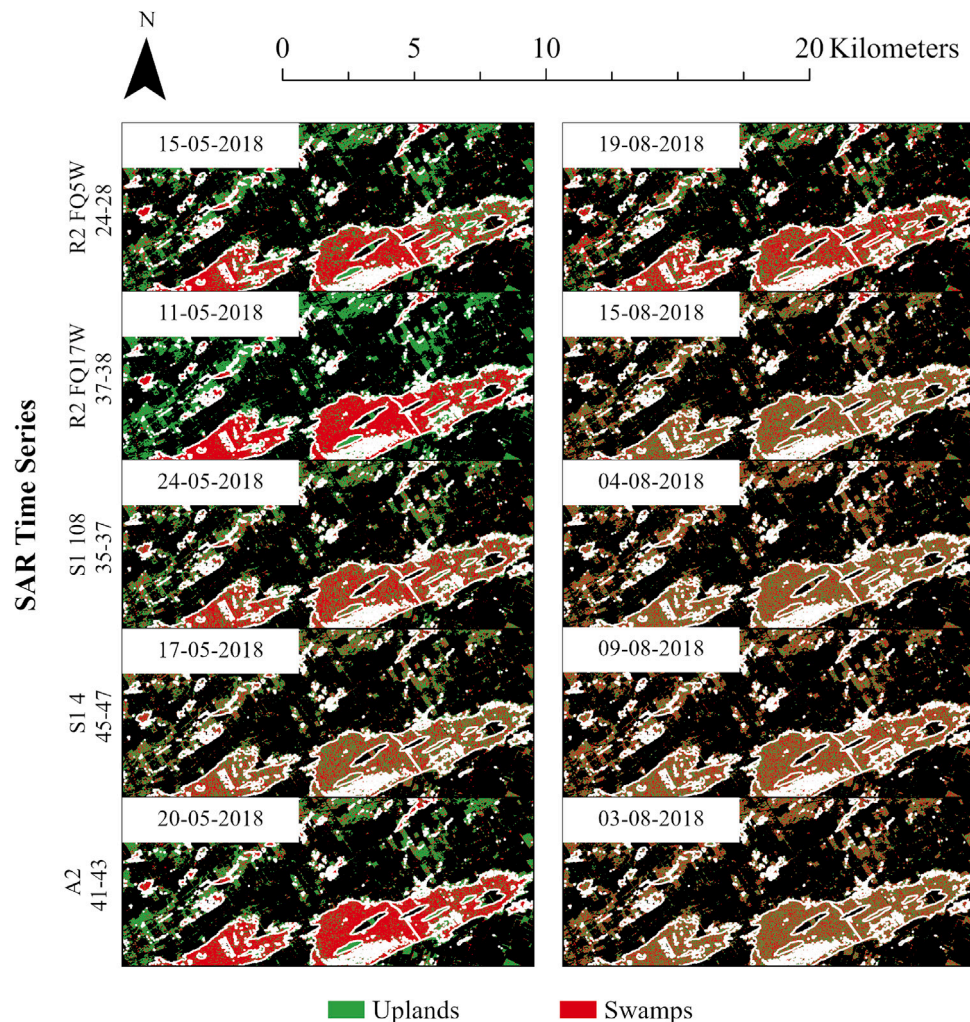


Fig. 9. Example classification results (one model run per time series) based on intensity derivatives (HH, HV, VH and/or VV polarization) for a select number of single SAR images (dates), trained using all 400 samples per class. For comparison, dates for the Radarsat-2 and Sentinel-1 time series correspond to the closest acquisitions to (1) the Alos-2 image acquired on May 20th, and (2) the Alos-2 image acquired on August 3rd.

apparent if: (1) results are not compared to other SAR sensors, and (2) if the data used for model training and validation are similarly biased toward sites where models perform similarly regardless of the SAR data that is used. For example, it is theorized that models may perform similarly in areas with relatively open and simple canopy structures. Therefore, having HH polarized data with a better NESZ, and or increasing polarimetric diversity may only offer advantages under certain scenarios.

Future work is needed to better understand the combined impact of SAR sensor and environmental characteristics for mapping and monitoring change in stands dominated by coniferous and mixed coniferous-deciduous trees and/or shrubs. Moreover, since all the swamps in this study area contained at least some open water there is also need to better understand the extent to which diffusion at the ground due to the presence of hummocks, sphagnum, and other vegetation, may result in an underestimation of the extent of swamps.

7. Conclusions

The study findings challenge the common preconception that longer wavelengths are preferred for distinguishing swamps from dry upland

forests and shrublands. Close scrutiny is therefore needed when selecting the type of SAR data that are used for a given application, or to temper the interpretation of results against biases that may not be readily apparent given limited and often biased training and validation data. While we have shown that images acquired before leaf flush are superior, we also found that including a DEM and its derivatives can partially compensate for use of sub-optimal SAR data.

CRedit authorship contribution statement

Sarah Banks: Conceptualization, Data curation, Formal analysis, Investigation, Methodology, Project administration, Visualization, Writing – original draft, Writing – review & editing. **Koreen Millard:** Supervision, Validation. **Laura Dingle-Robertson:** Supervision, Validation. **Jason Duffe:** Funding acquisition, Validation, Visualization.

Declaration of competing interest

The authors declare the following financial interests/personal relationships which may be considered as potential competing interests: Sarah Banks reports financial support, administrative support, article publishing charges, and writing assistance were provided by Environment and Climate Change Canada.

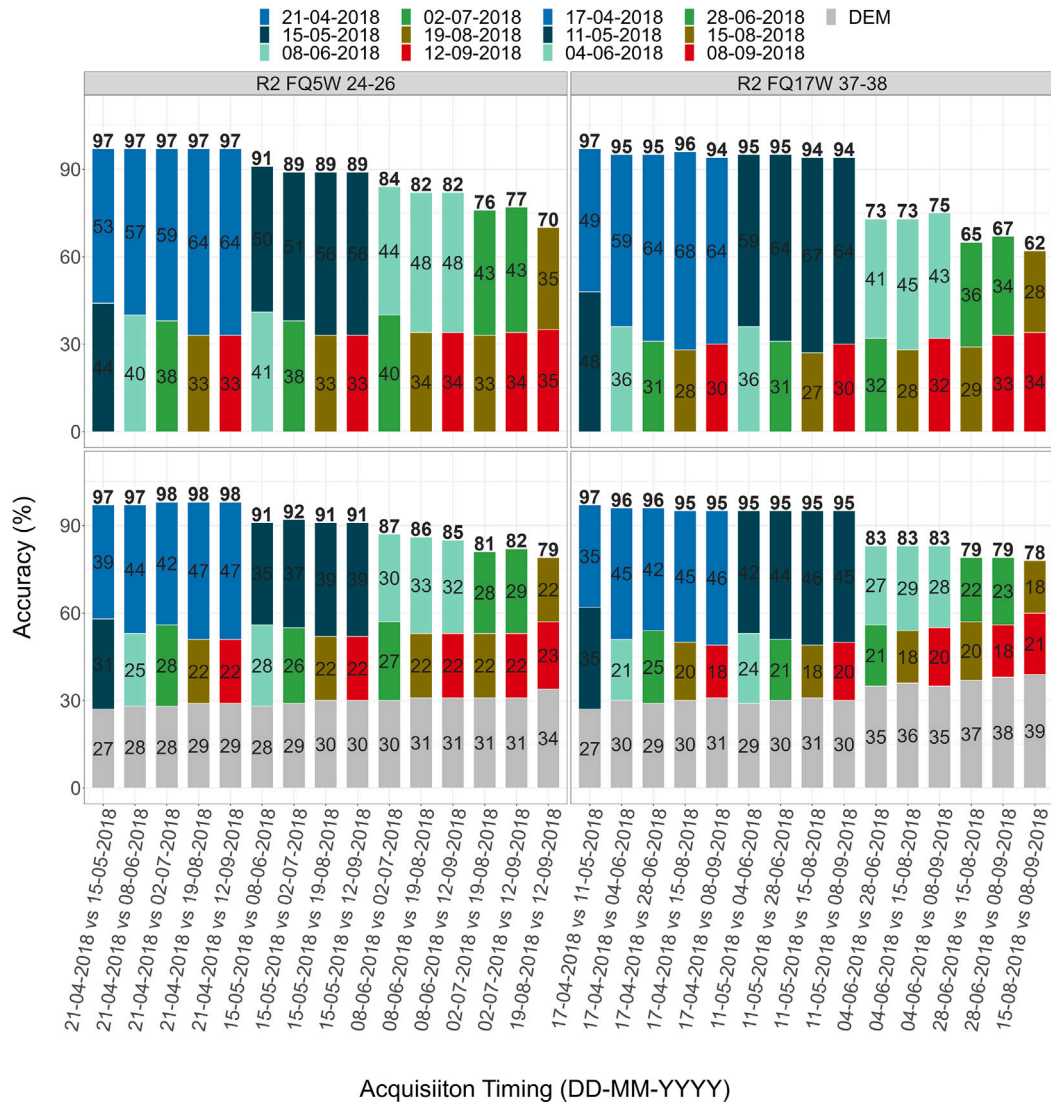


Fig. 10. Shapley values for grouped sets of Radarsat-2 variables (by SAR acquisition date and by DEM, topographic wetness (TWI) and slope (SLP) together) to demonstrate their relative importance to the independent overall accuracy (total bar height) of multiple Random Forest models (averaged across 100 runs). Shown above are all possible two-date combinations, classified alone (top row) and with a DEM and derivatives (bottom row).

Data availability

The authors do not have permission to share data.

Acknowledgements

The authors would like to express their gratitude to Dr. Frank Ahern for helping to interpret the results, for reviewing the manuscript

and offering valuable feedback to enhance its quality and readability. We also thank Robert Thompson and Ash Nassef for their assistance with docker, Patrick Kirby for writing the R code used to calculate the Shapley values, Dr. Amir Behnamian, Lori White, Dr. Zhaohua Chen, Taylor Harmer, Matt Giles, and Tom Giles for their assistance in planning and conducting field work. RADARSAT-2 Data and Products © Maxar Technologies Ltd.(2018) – All Rights Reserved. RADARSAT is an official mark of the Canadian Space Agency.

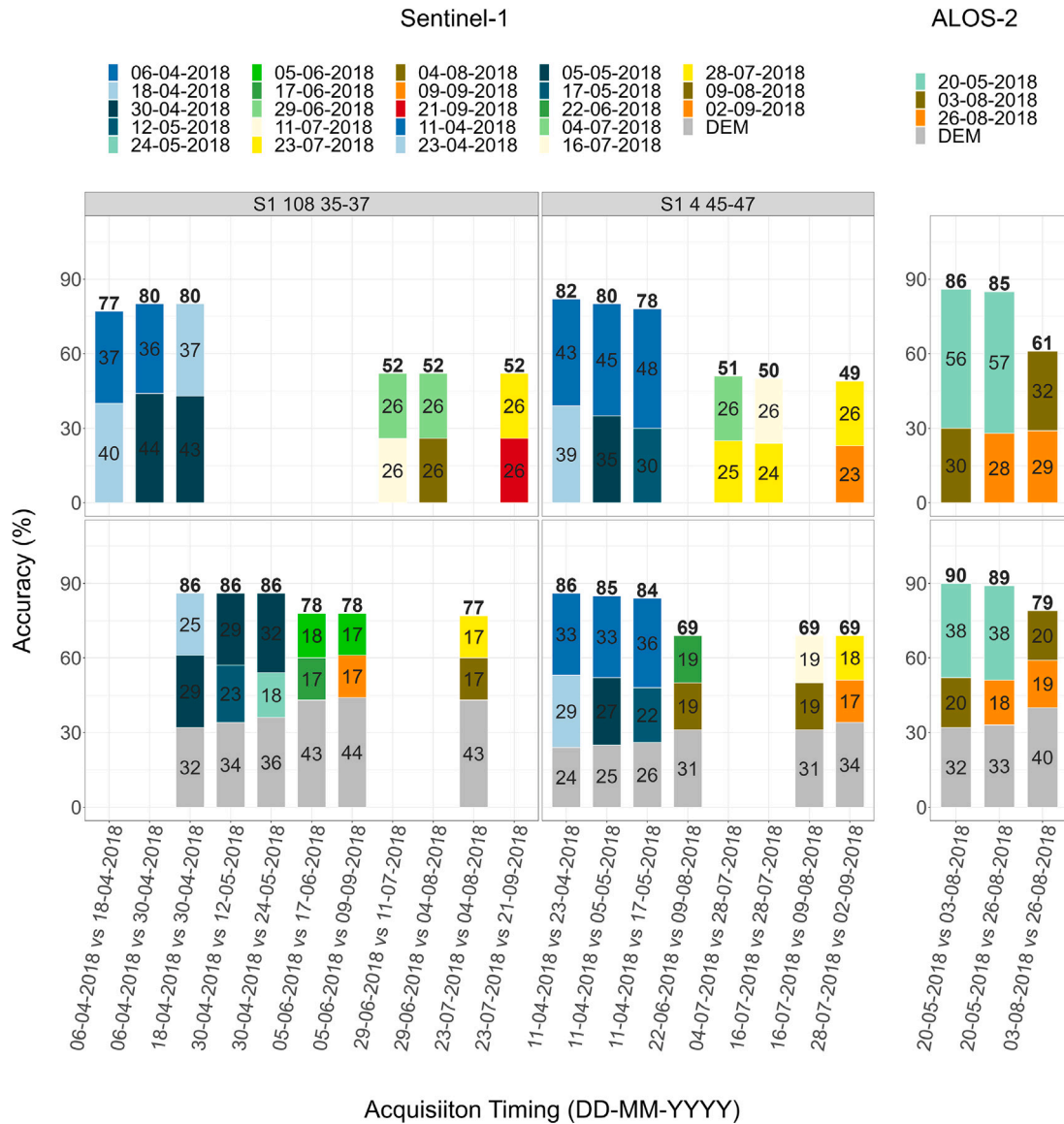


Fig. 11. Shapley values for grouped sets of Sentinel-1 and Alos-2 variables (by SAR acquisition date and by DEM, topographic wetness (TWI) and slope (SLP) together) to demonstrate their relative importance to the independent overall accuracy (total bar height) of multiple Random Forest models (averaged across 100 runs). For the Sentinel-1 time series, only the three models with the highest and the three models with the lowest accuracies are shown for brevity, while all possible two-date combinations are shown for Alos-2. Models above are for those classified alone (top row) and with a DEM and derivatives (bottom row).

References

- Ahern, F., Brisco, B., Battaglia, M., Bourgeau-Chavez, L., Atwood, D., Murnaghan, K., 2022. SAR polarimetric phase differences in wetlands: Information and mis-information. *Can. J. Remote Sens.* 1–19.
- Ahern, F., Brisco, B., Murnaghan, K., Lancaster, P., Atwood, D.K., 2018. Insights into polarimetric processing for wetlands from backscatter modeling and multi-incidence radarsat-2 data. *IEEE J. Sel. Top. Appl. Earth Obs. Remote Sens.* 11 (9), 3040–3050.
- Amani, M., Salehi, B., Mahdavi, S., Granger, J., Brisco, B., 2017. Wetland classification in newfoundland and labrador using multi-source SAR and optical data integration. *GISci. Remote Sens.* 54 (6), 779–796.
- Anfinsen, S.N., Dougeris, A.P., Eltoft, T.R., 2009. Estimation of the equivalent number of looks in polarimetric synthetic aperture radar imagery. *IEEE Trans. Geosci. Remote Sens.* 47 (11), 3795–3809.
- Atwood, D., Battaglia, M., Bourgeau-Chavez, L., Ahern, F., Murnaghan, K., Brisco, B., 2020. Exploring polarimetric phase of microwave backscatter from typha wetlands. *Can. J. Remote Sens.* 46 (1), 49–66.
- Banks, S., White, L., Behnamian, A., Chen, Z., Montpetit, B., Brisco, B., Pasher, J., Duffe, J., 2019. Wetland classification with multi-angle/temporal SAR using random forests. *Remote Sens.* 11 (6), 670.
- Belgiu, M., Drăguț, L., 2016. Random forest in remote sensing: A review of applications and future directions. *ISPRS J. Photogram. Remote Sens.* 114, 24–31.
- Bona, K.A., Hilger, A., Burgess, M., Wozney, N., Shaw, C., 2018. A peatland productivity and decomposition parameter database. *Ecology* 99 (10).
- Bona, K.A., Shaw, C., Thompson, D.K., Hararuk, O., Webster, K., Zhang, G., Voicu, M., Kurz, W.A., 2020. The Canadian model for peatlands (CaMP): A peatland carbon model for national greenhouse gas reporting. *Ecol. Model.* 431, 109164.
- Bourgeau-Chavez, L., Kasischke, E., Brunzell, S., Mudd, J., Smith, K., Frick, A., 2001. Analysis of space-borne SAR data for wetland mapping in virginia riparian ecosystems. *Int. J. Remote Sens.* 22 (18), 3665–3687.
- Bourgeau-Chavez, L.L., Lee, Y.M., Battaglia, M., Endres, S.L., Laubach, Z.M., Scarborough, K., 2016. Identification of woodland vernal pools with seasonal change PALSAR data for habitat conservation. *Remote Sens.* 8 (6), 490.
- Bourgeau-Chavez, L., Riordan, K., Nowels, M., Miller, N., 2004. Final report to the great lakes commission: Remotely monitoring great Lakes Coastal wetlands using a hybrid radar and multi-spectral sensor approach.
- Bourgeau-Chavez, L., Riordan, K., Powell, R., Miller, N., Nowels, M., 2009. Improving wetland characterization with multi-sensor, multi-temporal SAR and optical/infrared data fusion. *Adv. Geosci. Remote Sens.* 679–708.
- Breiman, L., 2001. Random forests. *Mach. Learn.* 45 (1), 5–32.
- Brisco, B., Ahern, F., Hong, S.-H., Wdowinski, S., Murnaghan, K., White, L., Atwood, D.K., 2015. Polarimetric decompositions of temperate wetlands at C-band. *IEEE J. Sel. Top. Appl. Earth Obs. Remote Sens.* 8 (7), 3585–3594.
- Brisco, B., Ahern, F., Murnaghan, K., White, L., Canisus, F., Lancaster, P., 2017. Seasonal change in wetland coherence as an aid to wetland monitoring. *Remote Sens.* 9 (2), 158.
- Brisco, B., Schmitt, A., Murnaghan, K., Kaya, S., Roth, A., 2013. SAR polarimetric change detection for flooded vegetation. *Int. J. Digit. Earth* 6 (2), 103–114.
- Bunting, M.J., Morgan, C.R., Bakel, M.V., Warner, B.G., 1998. Pre-European settlement conditions and human disturbance of a coniferous swamp in southern Ontario. *Can. J. Bot.* 76 (10), 1770–1779.
- Byun, E., Finkelstein, S.A., Cowling, S.A., Badiou, P., 2018. Potential carbon loss associated with post-settlement wetland conversion in southern Ontario, Canada. *Carbon Balance Manage.* 13 (1), 1–12.
- Canty, M., 2024. Change Detection with Multitemporal Polarimetric SAR Imagery. URL <https://github.com/mortcanty/SARDocker>.
- Cloude, S.R., Pottier, E., 1996. A review of target decomposition theorems in radar polarimetry. *IEEE Trans. Geosci. Remote Sens.* 34 (2), 498–518.
- Conradsen, K., Nielsen, A.A., Schou, J., Skriver, H., 2003. A test statistic in the complex wishart distribution and its application to change detection in polarimetric SAR data. *IEEE Trans. Geosci. Remote Sens.* 41 (1), 4–19.
- Conradsen, K., Nielsen, A.A., Skriver, H., 2016. Determining the points of change in time series of polarimetric SAR data. *IEEE Trans. Geosci. Remote Sens.* 54 (5), 3007–3024.
- Corcoran, J.M., Knight, J.F., Gallant, A.L., 2013. Influence of multi-source and multi-temporal remotely sensed and ancillary data on the accuracy of random forest classification of wetlands in Northern Minnesota. *Remote Sens.* 5 (7), 3212–3238.
- Costa, M., 2004. Use of SAR satellites for mapping zonation of vegetation communities in the amazon floodplain. *Int. J. Remote Sens.* 25 (10), 1817–1835.
- Costa, M.d.F., Novo, E.d., Ahern, F., Mitsuo, F., Mantovani, J., Ballester, M., Pietsch, R., 1998. The amazon floodplain through radar eyes: Lago grande de Monte alegre case study. *Can. J. Remote Sens.* 24 (4), 339–349.
- Dabhoor, M., Banks, S., White, L., Brisco, B., Behnamian, A., Chen, Z., Murnaghan, K., 2019. Comparison of compact and fully polarimetric SAR for multitemporal wetland monitoring. *IEEE J. Sel. Top. Appl. Earth Obs. Remote Sens.* 12 (5), 1417–1430.
- Davidson, S.J., Dazé, E., Byun, E., Hiler, D., Kangur, M., Talbot, J., Finkelstein, S.A., Strack, M., 2022. The unrecognized importance of carbon stocks and fluxes from swamps in Canada and the USA. *Environ. Res. Lett.* 17 (5), 053003.
- Dobson, M.C., Ulaby, F.T., Pierce, L.E., Sharik, T.L., Bergen, K.M., Kelndorfer, J., Kendra, J.R., Li, E., Lin, Y.-C., Nashashibi, A., et al., 1995. Estimation of forest biophysical characteristics in northern michigan with SIR-C/X-SAR. *IEEE Trans. Geosci. Remote Sens.* 33 (4), 877–895.
- Dugan, P., Dungan, P.J., 1990. Wetland Conservation: A Review of Current Issues and Required Action. IUCN.
- Engheta, N., Elachi, C., 1982. Radar scattering from a diffuse vegetation layer over a smooth surface. *IEEE Trans. Geosci. Remote Sens.* GE-20 (2), 212–216.
- Ford, J., Casey, D., 1988. Shuttle radar mapping with diverse incidence angles in the rainforest of Borneo. *Int. J. Remote Sens.* 9 (5), 927–943.
- Freeman, A., Durden, S.L., 1998. A three-component scattering model for polarimetric SAR data. *IEEE Trans. Geosci. Remote Sens.* 36 (3), 963–973.
- Genuer, R., Poggi, J.-M., Tuleau-Malot, C., 2010. Variable selection using random forests. *Pattern Recognit. Lett.* 31 (14), 2225–2236.
- Gesch, D.B., 1990. The derivation of a sub-canopy digital terrain model of a flooded forest using synthetic aperture radar. *Photogramm. Eng. Remote Sens.* 56 (8), 1155–1162.
- Golet, F.C., Larson, J.S., 1974. Classification of Freshwater Wetlands in the Glaciated Northeast, vol. 116, Bureau of Sport Fisheries and Wildlife, Fish and Wildlife Service, US
- Grenier, M., Demers, A.-M., Labrecque, S., Benoit, M., Fournier, R.A., Drolet, B., 2007. An object-based method to map wetland using RADARSAT-1 and landsat ETM images: test case on two sites in Quebec, Canada. *Can. J. Remote Sens.* 33 (sup1), S28–S45.
- Hall, J.V., Frayer, W., Wilen, B.O., 1994. Status of Alaska Wetlands. US Fish & Wildlife Service, Alaska Region.
- Henderson, F.M., Lewis, A.J., 2008. Radar detection of wetland ecosystems: a review. *Int. J. Remote Sens.* 29 (20), 5809–5835.
- Henry, J.-B., Chastanet, P., Fellah, K., Desnos, Y.-L., 2006. Envisat multi-polarized ASAR data for flood mapping. *Int. J. Remote Sens.* 27 (10), 1921–1929.
- Hess, L.L., Melack, J.M., 1994. Mapping wetland hydrology and vegetation with synthetic aperture radar. *Int. J. Ecol. Environ. Sci.* 20 (1–2), 74–81.
- Hess, L., Melack, J., 2003. Remote sensing of vegetation and flooding on magela creek floodplain (Northern Territory, Australia) with the SIR-C synthetic aperture radar. In: *Aquatic Biodiversity*. Springer, pp. 65–82.
- Hess, L.L., Melack, J.M., Filoso, S., Wang, Y., 1995. Delineation of inundated area and vegetation along the amazon floodplain with the SIR-C synthetic aperture radar. *IEEE Trans. Geosci. Remote Sens.* 33 (4), 896–904.
- Hess, L.L., Melack, J.M., Simonett, D.S., 1990. Radar detection of flooding beneath the forest canopy: a review. *Int. J. Remote Sens.* 11 (7), 1313–1325.
- Horritt, M., Mason, D., Cobby, D., Davenport, I., Bates, P., 2003. Waterline mapping in flooded vegetation from airborne SAR imagery. *Remote Sens. Environ.* 85 (3), 271–281.
- Imhoff, M., Story, M., Vermillion, C., Khan, F., Polcyn, F., 1986. Forest canopy characterization and vegetation penetration assessment with space-borne radar. *IEEE Trans. Geosci. Remote Sens.* GE-24 (4), 535–542.
- Kandus, P., Karszenbaum, H., Pultz, T., Parmuchi, G., Bava, J., 2001. Influence of flood conditions and vegetation status on the radar backscatter of wetland ecosystems. *Can. J. Remote Sens.* 27 (6), 651–662.
- Kasischke, E.S., Bourgeau-Chavez, L.L., 1997. Monitoring south florida wetlands using ERS-1 SAR imagery. *Photogramm. Eng. Remote Sens.* 63 (3), 281–291.
- Krohn, M.D., Milton, N., Segal, D.B., 1983. Seasat synthetic aperture radar (SAR) response to lowland vegetation types in eastern Maryland and Virginia. *J. Geophys. Res.: Oceans* 88 (C3), 1937–1952.
- Kuhn, M.A., Varner, R.K., Bastviken, D., Crill, P., MacIntyre, S., Turetsky, M., Walter Anthony, K., McGuire, A.D., Olefeldt, D., 2021. BAWLD-CH 4: a comprehensive dataset of methane fluxes from boreal and arctic ecosystems. *Earth Syst. Sci. Data* 13 (11), 5151–5189.
- Lang, M.W., Kasischke, E.S., Prince, S.D., Pittman, K.W., 2008a. Assessment of C-band synthetic aperture radar data for mapping and monitoring coastal plain forested wetlands in the Mid-Atlantic region, USA. *Remote Sens. Environ.* 112 (11), 4120–4130.
- Lang, M.W., Townsend, P.A., Kasischke, E.S., 2008b. Influence of incidence angle on detecting flooded forests using C-HH synthetic aperture radar data. *Remote Sens. Environ.* 112 (10), 3898–3907.
- Liaw, A., Wiener, M., et al., 2002. Classification and regression by randomforest. *R News* 2 (3), 18–22.
- Magagi, R., Bernier, M., Ung, C.-H., 2002. Quantitative analysis of RADARSAT SAR data over a sparse forest canopy. *IEEE Trans. Geosci. Remote Sens.* 40 (6), 1301–1313.
- Mahdavi, S., Salehi, B., Granger, J., Amani, M., Brisco, B., Huang, W., 2018. Remote sensing for wetland classification: A comprehensive review. *GISci. Remote Sens.* 55 (5), 623–658.
- Millard, K., Kirby, P., Nandlall, S., Behnamian, A., Banks, S., Pacini, F., 2020. Using growing-season time series coherence for improved peatland mapping: Comparing the contributions of sentinel-1 and RADARSAT-2 coherence in full and partial time series. *Remote Sens.* 12 (15), 2465.
- Millard, K., Richardson, M., 2013. Wetland mapping with LIDAR derivatives, SAR polarimetric decompositions, and LiDAR-SAR fusion using a random forest classifier. *Can. J. Remote Sens.* 39 (4), 290–307.

- Millard, K., Richardson, M., 2015. On the importance of training data sample selection in random forest image classification: A case study in peatland ecosystem mapping. *Remote Sens.* 7 (7), 8489–8515.
- Millennium Ecosystem Assessment, 2005. *Ecosystems and Human Well-Being: Wetlands and Water*. World Resources Institute.
- Milne, A., Horn, G., Finlayson, M., 2000. Monitoring wetlands inundation patterns using RADARSAT multitemporal data. *Can. J. Remote Sens.* 26 (2), 133–141.
- Ministry of Natural Resources, Forestry, 2014. *Ontario Wetland Evaluation System*. Tech. Rep., Ministry of Natural Resources and Forestry.
- Mitsch, W.J., Gosselink, J.G., 2015. *Wetlands*. John Wiley & Sons.
- Moreau, S., Bourrel, L., Bolivia, T., 1998. Hydrogeodynamics of the wetlands in the Bolivian. In: *Radarsat for Amazonia: Results of Proradar Investigations*. Canada Centre for Remote Sensing, Natural Resources Canada, p. 193.
- Muro, J., Canty, M., Conradsen, K., Hüttich, C., Nielsen, A.A., Skriver, H., Remy, F., Strauch, A., Thonfeld, F., Menz, G., 2016. Short-term change detection in wetlands using sentinel-1 time series. *Remote Sens.* 8 (10), 795.
- Muro, J., Strauch, A., Fitoka, E., Tompoulidou, M., Thonfeld, F., 2019. Mapping wetland dynamics with SAR-based change detection in the cloud. *IEEE Geosci. Remote Sens. Lett.* 16 (10), 1536–1539.
- Nandlall, S.D., Millard, K., 2019. Quantifying the relative importance of variables and groups of variables in remote sensing classifiers using shapley values and game theory. *IEEE Geosci. Remote Sens. Lett.* 17 (1), 42–46.
- National Wetlands Working Group, et al., 1998. *Wetlands of Canada*. Sustain. Dev. Branch Environ. Canada Ottawa.
- Olefeldt, D., Hovemyr, M., Kuhn, M.A., Bastviken, D., Bohn, T.J., Connolly, J., Crill, P., Euskirchen, E.S., Finkelstein, S.A., Genet, H., et al., 2021. The boreal–arctic wetland and lake dataset (BAWLD). *Earth Syst. Sci. Data* 13 (11), 5127–5149.
- Ontario Ministry of Natural Resources, Forestry, 2018. Ontario regulation 230/08, species at risk in Ontario list.
- Ormsby, J.P., Blanchard, B.J., Blanchard, A.J., 1985. Detection of lowland flooding using active microwave systems. *Photogramm. Eng. Remote Sens.* 51.
- Place, J.L., 1985. Mapping of forested wetland: Use of seasat radar images to complement conventional sources. *Prof. Geogr.*
- Pontone, N., Millard, K., Thompson, D.K., Guindon, L., Beaudoin, A., 2024. A hierarchical, multi-sensor framework for peatland sub-class and vegetation mapping throughout the Canadian boreal forest. *Remote Sens. Ecol. Conserv.*
- Pope, K.O., Rey-Benayas, J.M., Paris, J.F., 1994. Radar remote sensing of forest and wetland ecosystems in the central American tropics. *Remote Sens. Environ.* 48 (2), 205–219.
- Pouliot, D., Latifovic, R., Pasher, J., Duffe, J., 2019. Assessment of convolution neural networks for wetland mapping with landsat in the central Canadian boreal forest region. *Remote Sens.* 11 (7), 772.
- Rao, B., Dwivedi, R., Kushwaha, S., Bhattacharya, S., Anand, J., Dasgupta, S., 1999. Monitoring the spatial extent of coastal wetlands using ERS-1 SAR data. *Int. J. Remote Sens.* 20 (13), 2509–2517.
- Richards, J., Woodgate, P., Skidmore, A., 1987. An explanation of enhanced radar backscattering from flooded forests. *Int. J. Remote Sens.* 8 (7), 1093–1100.
- Riley, J., 1994. Peat and peatland resources of southeastern Ontario. Ontario geological survey miscellaneous paper no. 154.
- Schmullius, C., Evans, D., 1997. Review article synthetic aperture radar (SAR) frequency and polarization requirements for applications in ecology, geology, hydrology, and oceanography: A tabular status quo after SIR-C/X-SAR. *Int. J. Remote Sens.* 18 (13), 2713–2722.
- Shapley, L.S., 1997. A value for n-person games. In: *Classics in Game Theory*. Vol. 69, Princeton Univ Pr.
- Sokol, J., McNairn, H., Pultz, T., 2004. Case studies demonstrating the hydrological applications of C-band multipolarized and polarimetric SAR. *Can. J. Remote Sens.* 30 (3), 470–483.
- Stoler, A.B., Relyea, R.A., 2020. Reviewing the role of plant litter inputs to forested wetland ecosystems: leafing through the literature. *Ecol. Monogr.* 90 (2), e01400.
- Strobl, C., Boulesteix, A.-L., Zeileis, A., Hothorn, T., 2007. Bias in random forest variable importance measures: Illustrations, sources and a solution. *BMC Bioinform.* 8 (1), 1–21.
- Tiner, R.W., Kenenski, I., Nuerminger, T., Eaton, J., Foulis, D., Smith, G., Frayer, W., 1994. *Recent Wetland Status and Trends in the Chesapeake Watershed(1982–1989)*: Technical Report. U. S. Fish and Wildlife Service, Region 5 Hadley MA USA. 70, p. 1994.
- Townsend, P.A., 2001. Mapping seasonal flooding in forested wetlands using multi-temporal radarsat SAR. *Photogramm. Eng. Remote Sens.* 67 (7), 857–864.
- Townsend, P.A., 2002a. Estimating forest structure in wetlands using multitemporal SAR. *Rem. Sens. Environ.* 79 (2–3), 288–304.
- Townsend, P., 2002b. Relationships between forest structure and the detection of flood inundation in forested wetlands using C-band SAR. *Int. J. Remote Sens.* 23 (3), 443–460.
- Townsend, P.A., Foster, J.R., 2002. Assessing flooding and vegetation structure in forested wetlands using radarsat SAR imagery. In: *IEEE International Geoscience and Remote Sensing Symposium*. Vol. 2, IEEE, pp. 1171–1173.
- Townsend, P.A., Walsh, S.J., 1998. Modeling floodplain inundation using an integrated GIS with radar and optical remote sensing. *Geomorphology* 21 (3–4), 295–312.
- Townsend, P.A., Walsh, S.J., 2001. Remote sensing of forested wetlands: application of multitemporal and multispectral satellite imagery to determine plant community composition and structure in southeastern USA. *Plant Ecol.* 157 (2), 129–149.
- Ullmann, T., Banks, S.N., Schmitt, A., Jagdhuber, T., 2017. Scattering characteristics of X-, C-and L-band PolSAR data examined for the tundra environment of the Tuktoyaktuk Peninsula, Canada. *Appl. Sci.* 7 (6), 595.
- Ullmann, T., Schmitt, A., Jagdhuber, T., 2016. Two component decomposition of dual polarimetric HH/VV SAR data: Case study for the tundra environment of the Mackenzie Delta region, Canada. *Remote Sens.* 8 (12), 1027.
- Voormansik, K., Praks, J., Antropov, O., Jagomägi, J., Zalite, K., 2013. Flood mapping with TerraSAR-X in forested regions in Estonia. *IEEE J. Sel. Top. Appl. Earth Obs. Remote Sens.* 7 (2), 562–577.
- Wang, Y., Day, J., Sun, G., 1993. Santa Barbara microwave backscattering model for woodlands. *Int. J. Remote Sens.* 14 (8), 1477–1493.
- Wang, Y., Hess, L.L., Filoso, S., Melack, J.M., 1995. Understanding the radar backscattering from flooded and nonflooded amazonian forests: Results from canopy backscatter modeling. *Remote Sens. Environ.* 54 (3), 324–332.
- Wang, Y., Imhoff, M., 1993. Simulated and observed L-HH radar backscatter from tropical mangrove forests. *Int. J. Remote Sens.* 14 (15), 2819–2828.
- Webster, K., Bhatti, J., Thompson, D., Nelson, S., Shaw, C., Bona, K., Hayne, S., Kurz, W., 2018. Spatially-integrated estimates of net ecosystem exchange and methane fluxes from Canadian peatlands. *Carbon Balance Manage.* 13 (1), 1–21.
- Welsch, D.J., 1995. *Forested Wetlands: Functions, Benefits and the Use of Best Management Practices*, vol. 1, US Department of Agriculture, Forest Service, Natural Resources Conservation ...
- White, L., Brisco, B., Dabboor, M., Schmitt, A., Pratt, A., 2015. A collection of SAR methodologies for monitoring wetlands. *Remote Sens.* 7 (6), 7615–7645.
- White, L., Millard, K., Banks, S., Richardson, M., Pasher, J., Duffe, J., 2017. Moving to the RADARSAT constellation mission: Comparing synthesized compact polarimetry and dual polarimetry data with fully polarimetric RADARSAT-2 data for image classification of peatlands. *Remote Sens.* 9 (6), 573.
- Woodhouse, I.H., 2017. *Introduction to Microwave Remote Sensing*. CRC Press.
- Zedler, J.B., Kercher, S., 2005. Wetland resources: status, trends, ecosystem services, and restorability. *Annu. Rev. Environ. Resour.* 30, 39–74.